LICENCE TO McMASTER UNIVERSITY

This Thesis has been written
[Thesis, Project Report, etc.]

by Randy J. Meecham for
[Full Name(s)]
Undergraduate course number 4K06 at McMaster University under the supervision/direction of Dr. J.H. Crocket.

In the interest of furthering teaching and research, I/we hereby grant to McMaster University:

1. The ownership of 7 copy(ies) of this work;
2. A non-exclusive licence to make copies of this work, (or any part thereof) the copyright of which is vested in me/us, for the full term of the copyright, or for so long as may be legally permitted. Such copies shall only be made in response to a written request from the Library or any University or similar institution.

I/we further acknowledge that this work (or a surrogate copy thereof) may be consulted without restriction by any interested person.

J.H. Crocket
Signature of Witness, Supervisor

Randy J. Meecham
Signature of Student

April 26/90
date

(This Licence to be bound with the work)

A Mineralogical and Fluid Inclusion Study of Massive Sulphide Samples From the Juan de Fuca Ridge, Northeast Pacific Ocean

A MINERALOGICAL AND FLUID INCLUSION STUDY OF MASSIVE SULPHIDE SAMPLES FROM THE JUAN DE FUCA RIDGE, NORTHEAST PACIFIC OCEAN

by

RANDY JOHN MEECHAM

A Thesis

Submitted to the Department of Geology

in Partial Fullfillment of the Requirements for the

Degree Bachelor of Science

McMaster University

April, 1990

BACHELOR OF SCIENCE (geology), (1987) McMaster University, Hamilton, Ontario

TITLE: A Mineralogical and Fluid Inclusion Study of Massive Sulphide Samples from the Juan de Fuca Ridge, Northeast Pacific Ocean.

AUTHOR: Randy John Meecham

SUPERVISOR: Dr. J. H. Crocket

NUMBER OF PAGES: x, 76

ABSTRACT

In the past decade, sites of hydrothermal activity along the Juan de Fuca Ridge have gained a growing amount of attention. Increased sampling has provided the materials for more detailed studies, including those collected from Axial Seamount, a large shield volcano on the central portion of the ridge. Axial Seamount is host to at least three active vent sites, one of which, along the northwest caldera wall, consists of recently active eruptive-fissures and nearby chimney-like spires. A sampled spire from this location and samples from other vent areas are described using reflected and transmitted light techniques. They have been found to consist of the sulphide phases sphalerite, wurtzite, pyrite, marcasite, chalcopyrite, isocubanite, and galena. Jordanite and tetrahedrite-tennanite are also known to precipitate at these vent sites, but were not observed here. The most dominant non-sulphide minerals are amorphous silica and barite. Native sulfur, Fe and Mn oxides and a variety of sulfosalts may also be present. The complex textures in these samples reflect precipitation and growth from higher temperature fluids that are mixing with local ambient seawater. Fluid inclusions in sphalerite have revealed salinities in the 5.6 to 7.0 weight % NaCl range, with homogenization temperatures ranging from 214.8^{0}C to 269.4^{0}C. Temperatures of homogenization require pressure-corrections

between approximately 9.0^{0}C and 13.0^{0}C, to set-up a range of trapping temperatures that lie between 211.8^{0}C and 279.4^{0}C. Fluid inclusions are also found in wurtzite, barite, and amorphous silica however, these would yield no data.

Middle Valley is a sedimented rift valley that lies at the extreme north end of the Juan de Fuca Ridge. A number of hydrothermal sulphide mounds that lie atop the sediment pile have been sampled. The mineralogy is similar to that at Axial Seamount; however, the dominant sulphide phase at Middle Valley is pyrrhotite. Textural differences between the two sites are significant, a result of the traversing of hydrothermal fluids through a thick package of hemepelagic sediment at Middle Valley. Samples from Middle Valley are found to contain no measurable fluid inclusions in the sections available for study. Mineralogical and fluid inclusion studies are important methods that can be used to help solve the complex growth history of sulfides that are and have been accumulating at mid-ocean ridge vent sites.

ACKNOWLEDGEMENTS

I wish to greatfully acknowledge Dr. J. H. Crocket for the time he spent supervising this project and for his continual guidance and helpful criticism.

Thanks also to Mark Baknes for helping to familiarize myself with the various research equipment used during the course of the study.

I wish also to thank Jack Whorwood for his assistance with photographic work and Tom Bryner for allowing me use of the reflected light photographic equipment in the Materials Science and Engineering department.

Thanks to Len Zwicker for use of the various diamond saws in the rock-cutting room.

I would also like to acknowledge my room-mate, Bruce Willmer for allowing me use of his computer and various software and for the helpful discussions concerning thesis presentation.

Table of Contents

List of Figures

List of Plates

List of Tables

CHAPTER 1

GENERAL INTRODUCTION - STATEMENT OF PROBLEM

Several distinct zones of hydrothermal activity have been located along spreading centers of the Juan de Fuca Ridge in the northwestern Pacific ocean. In the past decade, insight as to the nature of these hydrothermally active zones has increased substantially with the succession of deep submersible dives, bottom photography, heat-flow surveys, acoustic imagery, swath bathymetry, seismic reflection profiling, magnetometer profiling and scientific analysis performed on collected samples.

In 1983, one such distinct zone was discovered in the caldera of Axial Seamount on the central Juan de Fuca Ridge, at approximate location $45^{0}57'N$, $130^{0}02'W$, by team members of the Canadian American Seamount Expedition (CASM), using the Canadian submersible PISCES IV (Scott 1985; CASM II 1985; Hannington and Scott 1985).

Another region of venting was discovered in a sediment filled submarine rift valley, called Middle Valley, at the northern extremity of the Juan de Fuca Ridge (Villinger and Davis 1984; Adshead, Bornhold, and Davis 1986; Goodfellow and Blaise 1988).

A number of samples were collected from points at or very close to the Axial Seamount hydrothermal vent sites

described above with the onset of numerous scientific expeditions in the 1980's. Dredge and core samples were taken at Middle Valley also. The results obtained and included in this thesis are based on work performed on polished sections numbered XL-2A1-A, XL-2A1-B, and XL-2A2 from sample number XL1720-2A; XL-2B from sample number XL1720-2B; and XL-3A from Scott's Pinnacle, all of which are from within the caldera of Axial Seamount, and MV-DR1, MV-DR2, and MV-DR3 from Middle Valley dredges MVDR02-01, MXDR02-05 and MVDR06-03 respectively. The samples were obtained by Dr. J. H. Crocket at McMaster University from colleagues at the Geological Survey of Canada in Ottawa. These sections were studied using reflected and transmitted light microscopy in order to determine the overall mineralogical and textural variations. The samples were scanned visually under transmitted light for fluid inclusions suitable for heating and freezing experiments. If homogenization temperatures and freezing point depression data can be determined, such data will serve to decipher the hydrothermal fluid chemistry and the history of mid-ocean ridge submarine exhalation.

A number of the samples from Axial Seamount displayed anomalously high gold contents as well as elevated concentrations of As, Sb, Pb, and Ag (Hannington et al. 1986). Gold-rich samples include a 160 kg, 1.7 metre high, 0.4 metre diameter, intact spire collected in 1984 (CASM II

1985), with gold values ranging as high as 6.7 ppm, averaging 4.9 ppm. Hannington et al. (1986) suggested that gold is initially preconcentrated from the high temperature (>300^{0}C) fluids along with Cu-Fe rich sulphides. The gold is believed to subsequently undergo remobilization by later, low temperature (<250^{0}C) fluids, sustained over longer periods, which allows for reconcentration of the gold into SiO_2-Ba-Zn rich precipitates close to the surface of the deposit (Hannington et al. 1986). Fluid inclusion analysis and petrological work should provide insight into the complex paragenesis that mid-ocean ridge massive sulphides commonly display. Information regarding fluid temperatures from samples of highest gold concentration may determine whether both high and low temperature processes, as advocated by Hannington et al. (1986), have occurred. If inclusions suitable for measurement by heating and/or freezing are found in more than one mineral phase, the thermal history will be useful for verifying texturally constructed paragenetical sequences in terms of the changing fluid chemistry. Such information, and that from other studies, should improve understanding as to the exact conditions under which these and other similar deposits have formed.

Previous work conducted on samples collected from vent sites along the Juan de Fuca Ridge began in the early 1980's, with the quantity of studies performed steadily growing.

Axial Seamount and Middle Valley have received considerable attention following their discovery in the mid-80's.

Fluid inclusion work includes that performed on samples taken from a hydrothermal silica-sulphate-sulphide spire collected from the caldera of Axial Seamount. Hannington and Scott (1988) and Hannington (1986) analyzed 67 two-phase fluid inclusions in coarse crystals of wurzite and determined uncorrected homoginization temperatures to lie in the range of 173^0 to 240^0C. Inclusions were also described as abundant in amorphous silica but not measurable due to leakage upon heating. Koski et al. (1984) noted minute two-phase fluid inclusions in wurzite at the southern Juan de Fuca Ridge, with possible filling temperatures in the range of 150^0 to 250^0C, although quantitative analyses were not reported. Styrt et al. (1981) reported that fluid inclusions in wurzite from a Zn sulphide-rich chimney from the East Pacific Rise at 21^0N latitude gave formation temperatures in the range of 280^0 to 285^0C. Le Bel and Oudin (1982) measured fluid inclusions in Zn sulphide from an inactive mound sample at 21^0N and found trapping temperatures to lie in the range 288^0 to 300^0C.

Previous mineralogical descriptions include a detailed classification and mineralogical/paragenetical scheme for samples collected along a southern portion of the Juan de Fuca Ridge by Koski et al. (1984) and Paradis et al. (1988) and for samples collected from the East Pacific Rise (Graham

et al. 1988). Hannington and Scott (1988) have included mineralogy and paragenesis in their discussion of the silica-sulphate-sulphide spire alluded to earlier. Hannington (1986) gives a detailed overview of the mineralogy and chemistry of other samples collected from Axial Seamount. A description of samples taken from sulphide mounds in Middle Valley was made by Davis et al. (1987) and Goodfellow and Blaise (1988).

CHAPTER 2

LOCATION AND PHYSIOGEOGRAPHY

2.1 Juan de Fuca Ridge

2.1.1 Location

The Juan de Fuca Ridge is located about 500 km off the northwest coast of the United States and is an approximately 500 km long segment of mid-ocean ridge, striking roughly 020^0. It is terminated to the south by the Blanco Fracture Zone which itself extends to the ESE, and to the north by the Sovanco Fracture Zone which extends to the WNW (Fig.2.1). Overall spreading rates for the Juan de Fuca Ridge are medium and have been estimated at 29 - 30 mm/yr (half rate); however, a significant portion of the ridge crest morphology is typical of a faster spreading centre, particularly towards the south. The ridge is generally characterized by a narrow, well-defined, symmetrical, axial valley, that averages 1-2 km in width along its length and lacks an extensive cover by sediments.

2.1.2 Mineralogy and Sampling

The Juan de Fuca Ridge is characterized by mid-ocean ridge ferrobasalt (Vogt and Byerly 1976). Clague and Bunch (1976) and Koski et al. (1984) discuss the production of ferrobasalt as a means of crystal fractionation of

FIGURE 2.1. Regional map of the Juan de Fuca Ridge and associated tectonic elements (from Goodfellow and Blaise 1988). Locations of Axial Seamount and Middle Valley are as shown.

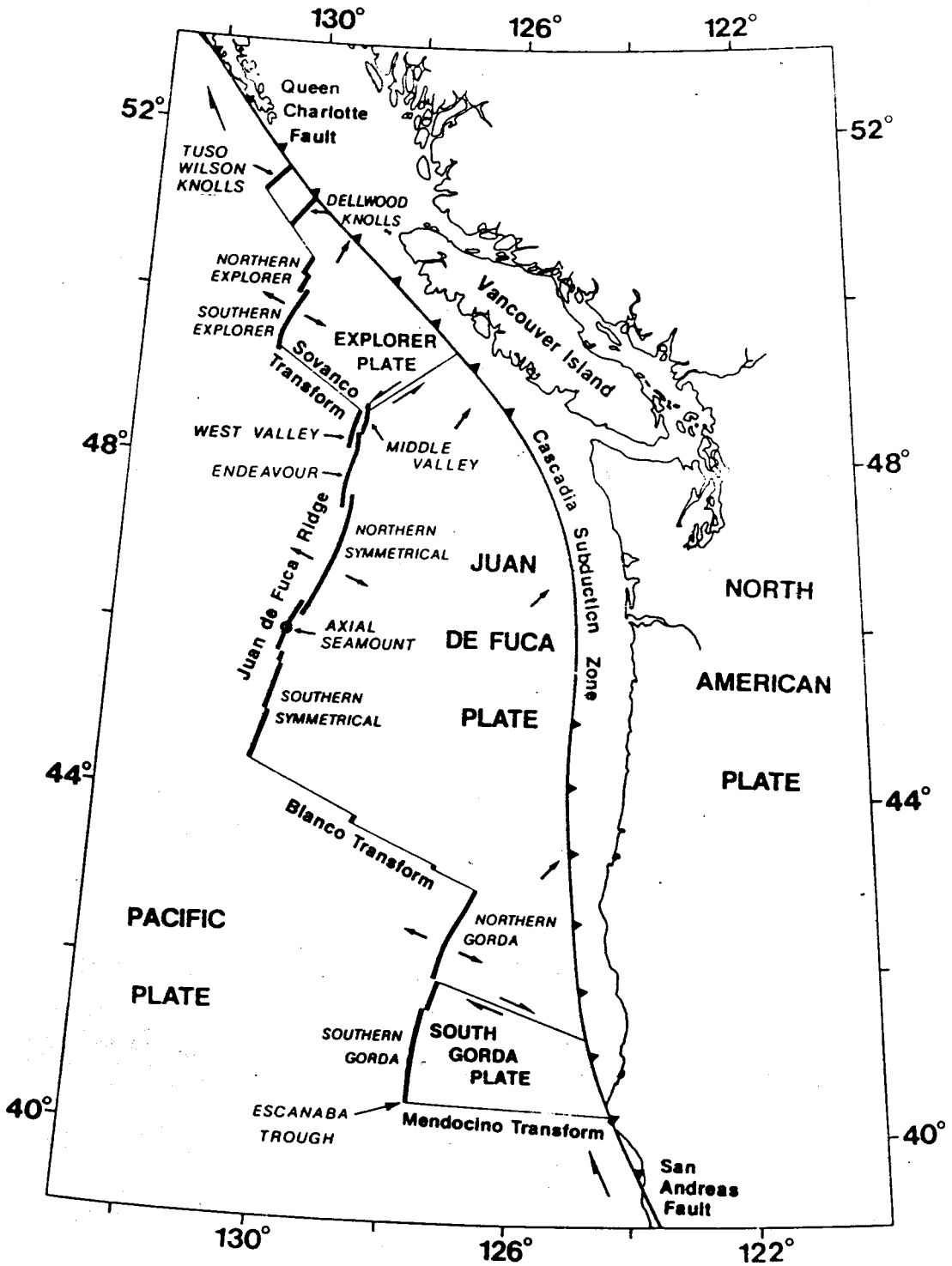
130°
126°
122°
52°
48°
44°
40°
Queen Charlotte Fault
TUSO WILSON KNOLLS
DELLWOOD KNOLLS
NORTHERN EXPLORER
SOUTHERN EXPLORER
EXPLORER PLATE
Sovanco Transform
WEST VALLEY
MIDDLE VALLEY
ENDEAVOUR
Juan de Fuca Ridge
NORTHERN SYMMETRICAL
AXIAL SEAMOUNT
SOUTHERN SYMMETRICAL
JUAN DE FUCA PLATE
Vancouver Island
Cascadia Subduction Zone
NORTH AMERICAN PLATE
Blanco Transform
PACIFIC PLATE
NORTHERN GORDA
SOUTHERN GORDA
SOUTH GORDA PLATE
ESCANABA TROUGH
Mendocino Transform
San Andreas Fault

plagioclase, clinopyroxene, and minor amounts of olivine in shallow magma reservoirs. Eaby and Clague (1982) consider that dredged sheet-flow and lobate-flow samples have textures similar to massive ferrobasalt with a glassy to microcrystalline groudmass containing a few phenocrysts of plagioclase, clinopyroxene, and olivine. Normark et al. (1983) have shown that the lavas located near hydrothermal vents in the axial valley are likely no more than a few hundred years old, which is indicated by the extreme rarity of palagonite on glassy basalt surfaces. Recovered basaltic fragments found near hydrothermal vents contain thin coatings of Fe and Mn-oxides on exposed surfaces.

A number of active and inactive vents sites are now well established along the Juan de Fuca Ridge, from Middle Valley at the extreme north, to areas along the southernmost segment of the ridge. Sulphide sampling along the Juan de Fuca Ridge includes those collected from the southern Juan de Fuca Ridge (Normark et al. 1982; Koski et al. 1984; USGS Juan de Fuca Ridge Study Group 1986), from Axial Seamount (Malahoff et al. 1984; Malahoff 1985; CASM Research Group 1985; ASHES Expedition 1986), from the Endeavor segment (Kingston and Delaney 1983; MERGE Group 1984; Hammond et al. 1983; Tivey and Delaney 1986), and at Middle Valley (Adshead 1987; Davis et al. 1987; Goodfellow and Blaise 1988).

2.2 Axial Seamount

2.2.1 Location

Axial Seamount is a large shield volcano located at the intersection of the Cobb-Eickelberg Seamount Chain and the Juan de Fuca ridge crest at approximate location $45^0$59'N, $130^0$03'W (Fig.2.1). The ridge reaches a minimum depth of 1490 m here, compared to depths ranging from 2200 to 2700 m along the flanks of the seamount. The summit of this broad edifice consists of an approximately 21 km^2 steep-walled caldera which is topographically flat-floored. The dimensions of the caldera are approximately 7 km by 3 km, with the long axis striking at about 340^0. The caldera floor lies at a depth of roughly 1570 m, with walls sometimes reaching 140 m in height. The southeastern side of the caldera has been breached and covered by large sheet flows which spread out to give a fan-shaped bathymetric profile (Fig.2.2a).

2.2.2 Vent Site

Hydrothermal vent fields and a small sulphide deposit were discovered along the north wall of the caldera by the Canadian deep-diving submersible PISCES IV (Canadian American Seamount Expedition (CASM II) 1985). This zone of active

FIGURE 2.2a. SEABEAM bathymetric map of the Axial Seamount Caldera (from CASM II 1985; Grasty et al. 1988). Isobaths are labelled at 100 m intervals. The location of three main vent fields are shown. Samples in this study come from the CASM and PISCES vent fields.

FIGURE 2.2b. Generalized geologic map of the CASM vent site (Fig.2.2a; from Hannington and Scott 1988). Shown are the various lava morphologies, eruptive fissures, caldera wall, and the sample locations. Cross-section A-B passes through the new and the old fissures and indicates the location of the sulphide deposit.

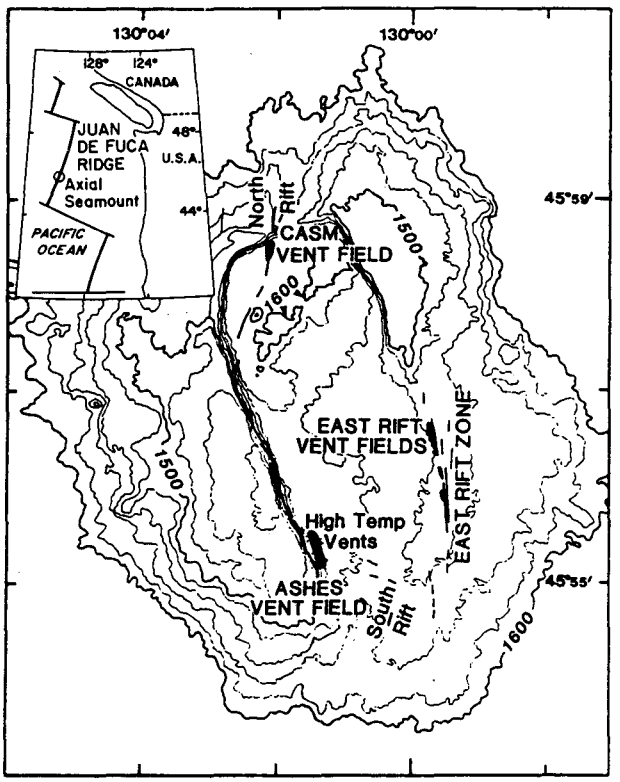
130°04′
130°00′
128°
124°
CANADA
JUAN DE FUCA RIDGE
Axial Seamount
48°
U.S.A.
44°
PACIFIC OCEAN
North Rift
CASM VENT FIELD
1500
1600
45°59′
EAST RIFT VENT FIELDS
EAST RIFT ZONE
High Temp Vents
ASHES VENT FIELD
South Rift
45°55′

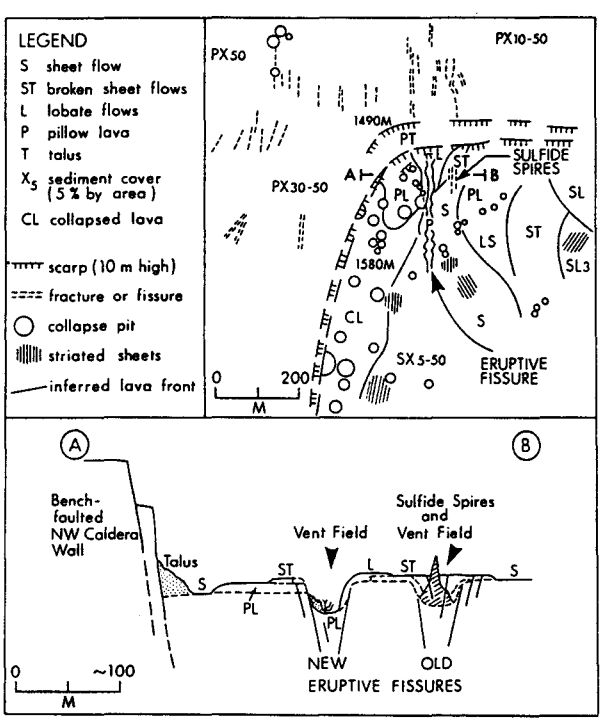
LEGEND
S sheet flow
ST broken sheet flows
L lobate flows
P pillow lava
T talus
X5 sediment cover (5 % by area)
CL collapsed lava
scarp (10 m high)
fracture or fissure
collapse pit
striated sheets
inferred lava front
PX50
PX10-50
PX30-50
1490M
1580M
PT
SULFIDE SPIRES
SL
SL3
LS
ST
PL
CL
SX5-50
ERUPTIVE FISSURE
0
200
M
A
B
Bench-faulted NW Caldera Wall
Talus
Vent Field
Sulfide Spires and Vent Field
L
NEW ERUPTIVE FISSURES
OLD
~100

venting is associated with abundant north-south trending fissures which emanate from the caldera's north wall and display the effects of active spreading along the central ridge axis which intersects the caldera obliquely. An eruptive fissure extends along the floor of the caldera from the northwest wall for roughly 300 m. This larger eruptive fissure coalesces from the smaller fissures in the caldera wall, which themselves range from 2 to 10 m in width and from 1 to 20 m in depth (Fig.2.2b). The fissure consists of seven overlapping collapse-structures cut by a central cleft. Three of the collapse pits are occupied by warm water vents (Hannington et al. 1986; Hannington and Scott 1988). Lobate lavas and fresh pillows occupy the margins of the fissure, while the bulk of the caldera floor is covered by sheet flows and collapsed lava ponds. The young age of these lava flows is indicated by the thin cover of pelagic sediments (< 5-10%) close to the eruptive fissure as opposed to thicker cover outside the caldera walls. Collapsed lava and draped lava on the fissure walls also lend evidence to the relatively young age of these flows.

A number of warm water vents occupy at least three of the collapsed structures within the eruptive fissure (Hannington et al. 1986; Hannington and Scott 1988). The vents occur either along the walls of the fissure or at its base, in areas where basaltic material has fractured

allowing hydrothermal fluids to escape. The hydrothermal fluids released from these fractures have been measured at < 35^0C, with ambient seawater at about 1.5^0 to 2.0^0C. The sulphide deposits resulting from active venting along the main eruptive fissure are considered immature (Hannington et al. 1986).

To the east, 40 or 50 m from the main eruptive fissure, lies a 30 m long fracture zone, which is an older eruptive fissure that has been partially buried by recent sheet flows (Fig.2.2b). A mature silica-sulphide deposit occurs along this narrow fracture zone which trends in a north-south direction. Three sulphide-sulphate chimneys, each about 12 m in height were discovered here, and a smaller 1.7 m high spire was sampled. Further details concerning the morphology of the seamount and caldera are noted by the Canadian American Seamount Expedition (CASM II) (1985) and by Hannington and Scott (1988).

2.3 Middle Valley

2.3.1 Location

Middle Valley is a sedimented, fault-bounded rift valley which lies at the extreme northern end of the Juan de Fuca Ridge (Fig.2.1). Sediment thicknesses within the valley range up to 1500 m and can be quite variable from the valley margins to the centre. Middle Valley has been filled mainly

by terrigenous sediments consisting of turbidite units of variable thickness interbedded with hemipelagic sediments as shown nicely by seismic reflection profiles. The filling of the valley by such a thick package of terrigenous sediments is in direct accord with its proximity to the continental shelf margin. As a result, sediment thickness also increases towards the north of the valley, which is closest to the source of the sediment flux. Spreading half rates for the Juan de Fuca Ridge have already been noted as typical of a medium to fast spreading center. However, at Middle Valley and a few other areas, spreading rates are slower. Slower rates may simply reflect somewhat different tectonics at the north extremity of the ridge possibly related to its proximity to a major transform fault (The Sovanco Fracture Zone), or a lack of a sufficient magma supply (Davis et al. 1987).

2.3.2 Vent Site

A number of mounds were found to exist along the eastern side of Middle Valley in 1983 by high-resolution acoustic imagery, swath bathymetry (Fig.2.3a), and seismic profiling studies (Fig.2.3b). The mounds are up to 1000 m across and rise to 60 m above the surrounding valley floor in some cases. These mounds, which are believed to be hydrothermal in origin, are located in an area where the sediment is approximately

FIGURE 2.3a. SEABEAM bathymetric map of Middle Valley (from Goodfellow and Blaise 1988) showing areas of high heat-flow and seismic reflection profile from A-B.

FIGURE 2.3b. Seismic reflection profile across Middle Valley, section A-B (Fig.2.3a). (Goodfellow and Blaise 1988).

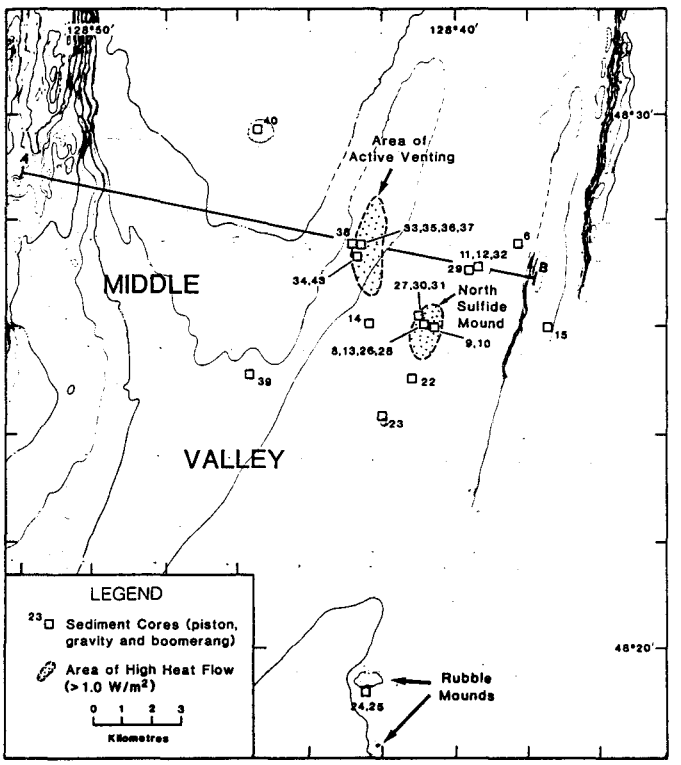
128°50'
128°40'
48°30'
48°20'
Area of Active Venting
MIDDLE
VALLEY
North Sulfide Mound
Rubble Mounds
LEGEND
Sediment Cores (piston, gravity and boomerang)
Area of High Heat Flow (> 1.0 W/m²)
0 1 2 3
Kilometres

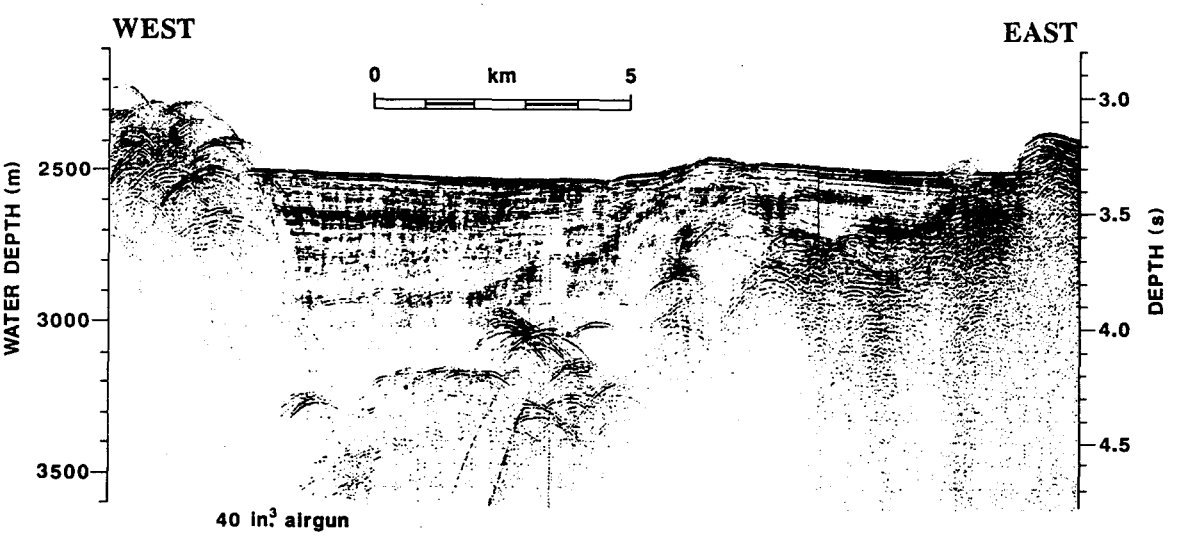
WEST
EAST
0 km 5
WATER DEPTH (m)
2500
3000
3500
DEPTH (s)
3.0
3.5
4.0
4.5
40 in.³ airgun

300 m thick, at a distance of 3 or 4 km west of the eastern valley-bounding normal fault scarp.

A total of eight mounds have been identified at this location. Seismic profiles show the mounds are layered, which is believed to be a reflection of sulphide layering as opposed to igneous sills since the area has been inactive magmatically over the last 50,000 years. Multi-penetration heat-flow profiles across these mounds have shown that they are associated with significant heat-flow anomalies. This observation, along with further evidence, has led to the acceptance of these mounds as hydrothermal in origin. The sediment pile acts as an impermeable cap on the ridge crest hydrothermal vents, which along with a number of other contributing factors, leads to the possibility that major sulphide deposits are present in Middle Valley.

A more detailed discussion of this study site is provided by Davis et al. (1987) and by Goodfellow and Blaise (1988).

CHAPTER 3

MINERALOGY AND TEXTURAL DESCRIPTIONS

3.0 Introduction - Petrography

Massive sulphide samples from vent sites along the Juan de Fuca Ridge have been petrographically described in some detail by others, both megascopically as well as microscopically. A detailed mineralogical classification of sulphide samples from the southern Juan de Fuca Ridge is given by Koski et al. (1984). His study serves well as a reference to describe samples from this area of the ridge as well as other vent sites along the ridge, since major mineralogical and textural similarities exist between sulphide samples from most ridge crests. Other important descriptions of seafloor sulphide samples from Axial Seamount have been made by Hannington (1986) and Hannington and Scott (1988). Davis et al. (1987) and Goodfellow and Blaise (1988) have provided detailed descriptions of dredge and core samples from sulphide mounds at Middle Valley. Many of the samples from the Juan de Fuca Ridge are texurally, mineralogically, and paragenetically similar, thus making it relatively easy to recognize the obvious differences that exist between similar samples from different sites. As descriptive documentation and other work continues, genetic models for the various deposits will be revised. The genetic

controls that cause these various sites to differ, or to assimilate, will, with continuing efforts, become more precisely known.

The following descriptions serve to document some of those samples from the vent sites studied in this thesis. Note that many of the textures and mineralogy described in the following section are not always visible in the photomicrographs since the scale is often too small or too large for these features to be seen. Descriptions representing the overall nature of the section are given and photomicrographs of every area can obviously not be shown.

3.1 Axial Seamount

3.1.1 Sample XL1720-2A

Three polished thin sections were cut from sample XL1720-2A, labelled XL-2A1-A, XL-2A1-B, and XL-2A2. The mineralogy and textures observable in transmitted and reflected light are described below.

The dominant mineral phases in sections numbered XL-2A1-A and XL-2A1-B are Zn sulphide and Fe sulphide. A wide wavy band of colloform sphalerite and marcasite runs across section A, which emphasizes the layered nature of these sulphide aggregates. Large scale growth banding is evident in each of the two sections and is best viewed under low magnification or with a hand-lens.

Multiple growth bands are visible at the microscopic level within the regions of colloform sphalerite and marcasite, often with delicate fine-scale alternating bands of Zn sulphide and Fe sulphide being very well developed (Fig.3.1a). These large bands of sphalerite often contain numerous minute blebs of chalcopyrite (Fig.3.1b), a feature described as "chalcopyrite disease" (Koski et al. 1984). Heterogeneities due to Cu-Fe-S content within sphalerite have been described for samples from the East Pacific Rise (Scott 1983). This may be, in part, the cause of opacity within cores of sphalerite grains as viewed in transmitted light. This phenomenon is also common to the sphalerite of Kuroko ores, such as those described by Barton (1978). Tiny inclusions of a pale yellow sulphide found within colloform cores of sphalerite have been described in samples from the southern Juan de Fuca Ridge (Koski et al. 1984).

A few of the larger grains of chalcopyrite exibit isotropic cores which are likely due to isocubanite which forms an intermediate solid solution pair with chalcopyrite. Subhedral grains of chalcopyrite can be found distributed within interstices of well developed wurtzite crystals or along the boundaries of zones consisting mainly of granular sphalerite. The proportion of Cu-Fe sulphide to other sulphide minerals is minor.

Trace amounts of galena occur as subhedral grains and

FIGURE 3.1. Photomicrographs of typical textures for Axial Seamount massive sulphides (sample XL1720-2A). Scale bars are in micrometers. A) Colloform growth patterns of Fe and Zn sulphides, with weakly developed dendrites of sphalerite. Gangue minerals interstitial to the sulphides are primarily amorphous silica and anhydrite. B) Cu-Fe sulphides in sphalerite illustrating "chalcopyrite disease" and growth bands of Fe sulphide. C) Dendritic growth of pyrite, and sphalerite with local barite crystals. D) Dendritic sphalerite bordering clusters of wurtzite crystals.

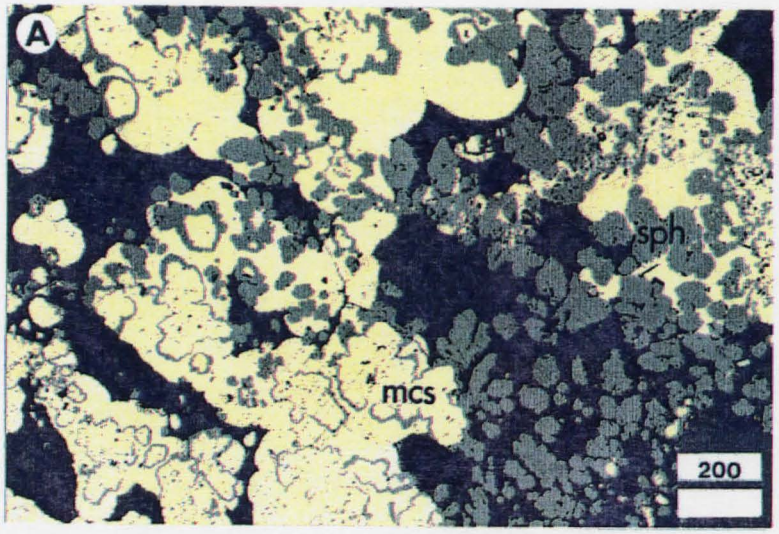
A
sph
mcs
200


C
200

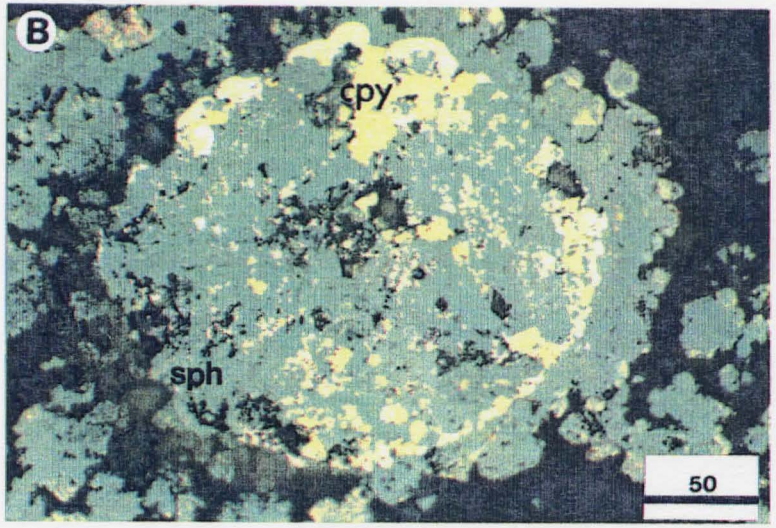
B
cpy
sph
50

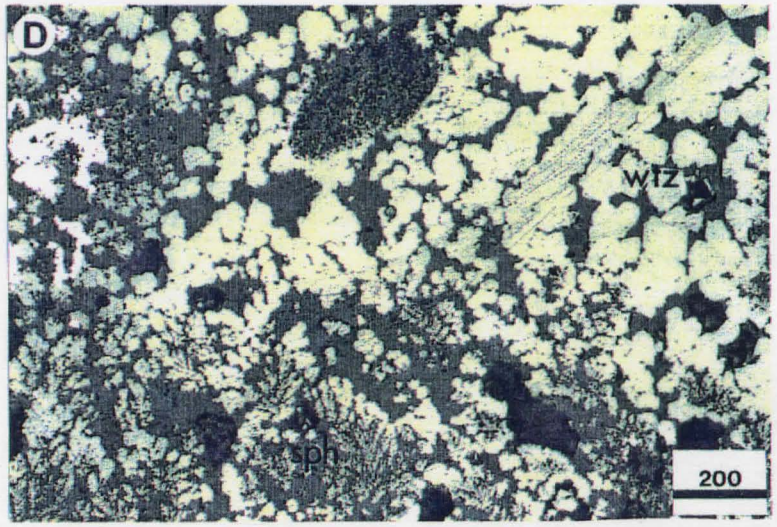
D
wtz
200

usually occur along the margins of colloform sphalerite. The galena crystals are usually seen projecting from the most outwardly growth surfaces of the colloform masses but, it is thought that those with deeper roots are perhaps representative of late-stage crytallographic extentions of previously formed dendrites (Koski et al. 1984). Jordanite ($Pb_4As_2S_7$) may be present also, however, a positive optical identification could not be made for this mineral.

Apart from the massive zone of colloform material, there are other textures indicative of open space growth. Beautiful dendritic growth patterns are formed by colloform sphalerite, and by colloform pyrite sometimes with associated marcasite (Fig.3.1c,d). Dendrites often conceal growth rings of their own as layers of Fe sulphide are interspersed with sphalerite, and maintain a consistent orientation with growth surfaces lying convex towards the surface of the colloform growth. Tapered hexagonal crystals of wurtzite occur in clusters usually lying in close proximity to the dendrites (Fig.3.2a).

Large areas of the XL1720-2A sections are occupied by subhedral to cubic forms of pyrite which often occur as individual grains but sometimes can form aggregates or clusters which conform to and help to generate the overall banding in the sample. Pyrite often displays a wide variety of atoll structures.

Large open pores are often lined by a narrow continuous

FIGURE 3.2. Photomicrographs of common textures in sample XL1720-2A. Scale bars in micrometers. A) Hexagonal wurtzite crystals growing within an open cavity filled by amourphous silica. B) Open cavity, possibly an abandoned feeder-channel, rimmed by Zn sulphides. Also zones of euhedral pyrite. C) Mantled worm tube casts with abundant wurtzite and anhydrite. D) Rosettes of barite set within an open cavity.

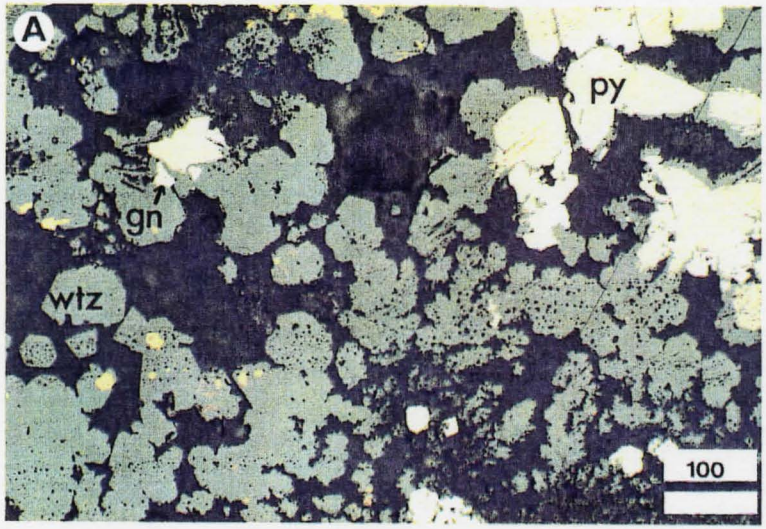
A
py
gn
wtz
100

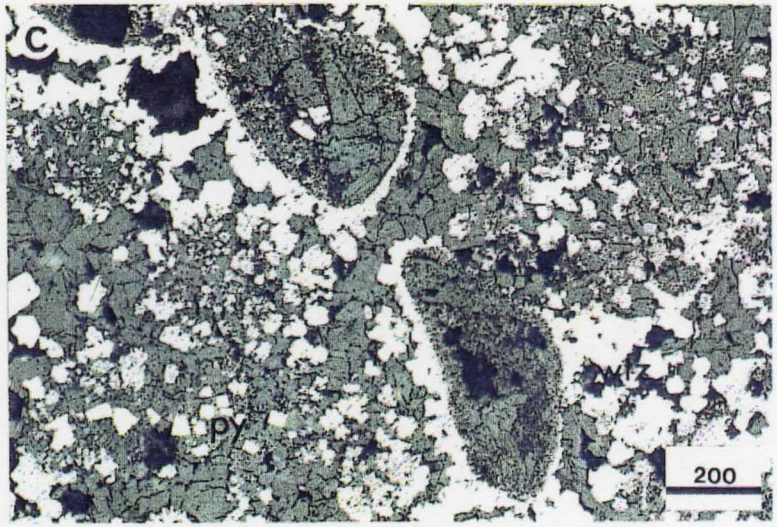
C
py
wtz
200

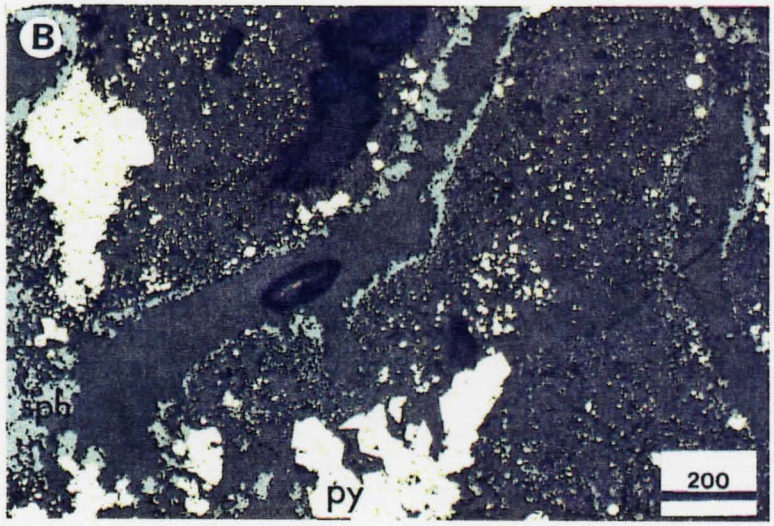
B
sph
py
200


D
sph
ba
200

band of sphalerite. These textural features are likely the result of abandoned feeder-channels or worm tube casts. The interior of these rounded or elongate voids have been infilled with anhydrite which may crystallize as quite large plates (Fig.3.2b,c). Fibrous bundles of amorphous silica and beautiful radiating rosettes of barite crystals (Fig.3.2d) are seen on polished surfaces under transmitted light in a few areas. Barite and amorphous silica can best be observed along open pores where opaque minerals are absent. The two minerals can be found throughout the two sections, usually in smaller quantities with less impressive textures.

A third section cut from sample XL1720-2A (section XL-2A2) displays many similar textures to sections XL-2A1-A and XL-2A1-B described above including large scale banding or layering. Intricate growth bands within Zn sulphide and Fe sulphide are visible within subhedral granular crystals and in rounded masses of colloform material. Colloform Fe sulphide forms narrow bands around the masses of colloform sphalerite from place to place, but as a whole, colloform sphalerite and pyrite are much less prominent in this section.

Virtually all of the granular pyrite is concentrated in a narrow band towards one end of the section. These grains appear to be singular and are anhedral to subhedral in habit, some containing small colloform cores which are ringed by sphalerite. There are also a few scattered minute grains of

pyrite distributed throughout the rest of the section, sometimes displaying cubic crystal outlines.

Most of the section is occupied by wide zones of densely packed anhedral to subhedral grains of sphalerite. The few scattered grains of pyrite that are interspersed within the Zn sulphide in these zones are much smaller by comparison. Often these wide regions of Zn sulphide consist of the largest grains seen (up to 1 mm)(Fig.3.3a). Under transmitted light, a few zones are found in which the Zn sulphide will transmit light, revealing light bronze coloured rims with slightly darker, copper-coloured cores. This may be attributed to the presence of greater quantities of iron in the crystal structure of sphalerite, towards the core in these grains, a feature also common to crystals of wurzite and colloform sphalerite from a nearby hydrothermal spire (Hannington and Scott 1988). A variety of textural observations, including crystal habit, compactness and quantity of grains, indicates that the sulphide phase in question here is shalerite. These large grains of sphalerite contain multiple specks of chalcopyrite, indicating "chalcopyrite disease" throughout this sample. Replacement of sphalerite by Cu-Fe sulphides is significant in these large grains. The importance of these large grains of sphalerite will be made clear in chapter 4 when fluid inclusion analysis of the sample is discussed.

Wurtzite crystals with hexagonal prismatic outlines are present in this section also, but are restricted to areas of open space, such as along pores or within wide cavities (Fig.3.3b). Wurzite accounts for roughly 20% of the total volume of Zn sulphides in this sample. Greater proportions (30%) have been determined by petrography and X-ray diffraction scans in samples from Scott's Pinnacle (Hannington and Scott 1988). Wurzite is common also to other ridge crest sulphide deposits such as the Southern Juan de Fuca Ridge and at 21^0N (Oudin 1981, 1983a; Koski et al. 1984; Haymon and Kastner 1981). Wurtzite is commonly regarded as a high temperature polymorph of sphalerite, which inverts univariantly to sphalerite as a function of sulfur fugacity and temperature (Scott and Barnes 1972).

Sphalerite and pyrite are also found as aggregates of small grains clustering around feeder-channels and worm tube casts (Fig.3.3c).

Barite, amourphous silica, and anhydrite are present as in sections XL-2A1-A and XL-2A1-B, but are less widespread in this section, probably due to the orientation of the section. Nevertheless, radiating clusters of barite are visible in a few areas, but as much smaller grains. Anhydrite has again filled the bulk of the feeder channels and amourphous silica is widely distributed within and along the margins of the many variable sized pores.

FIGURE 3.3. Photomicrographs of textures commonly found in sample XL1720-2A (A,B,C) and sample XL1720-2B (D). Scale bars are in micrometers. A) Coarse-grained sphalerite crystals with inclusions of Cu-Fe sulphides. B) Euhedral to subhedral crystal of wurtzite. C) Fine granular pyrite and sphalerite along abandoned feeder-channel. D) Large euhedral to subhedral crystals of wurtzite and growth banded Fe sulphides.

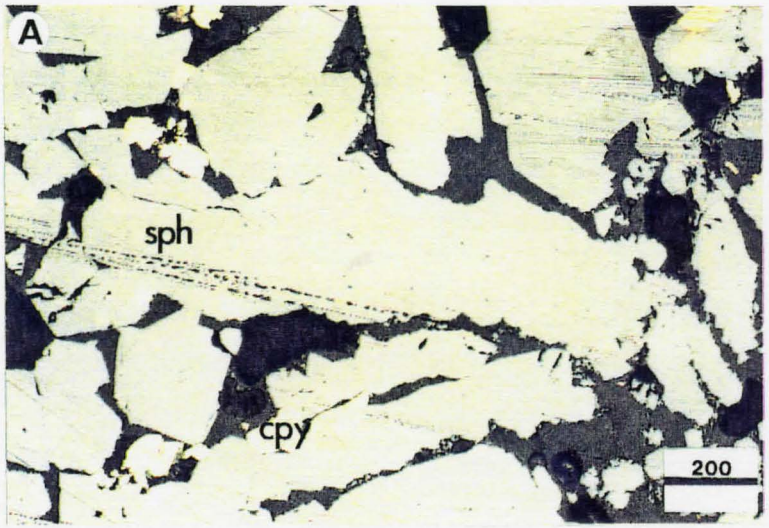
A
sph
cpy
200

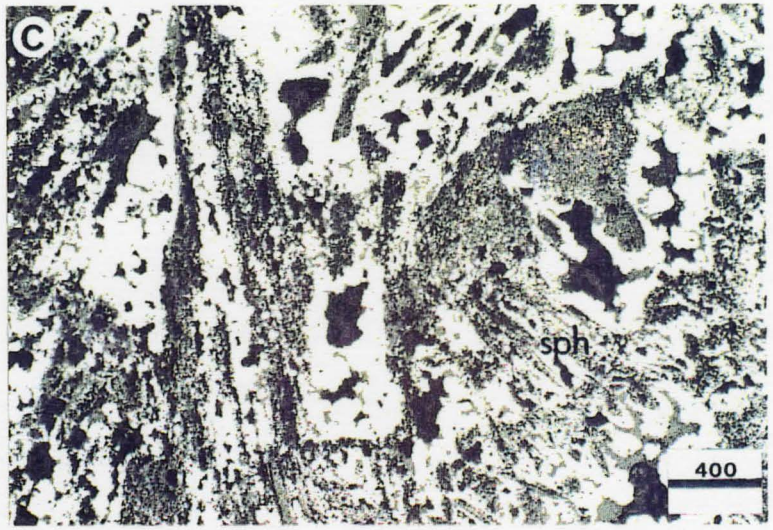
C
sph
400

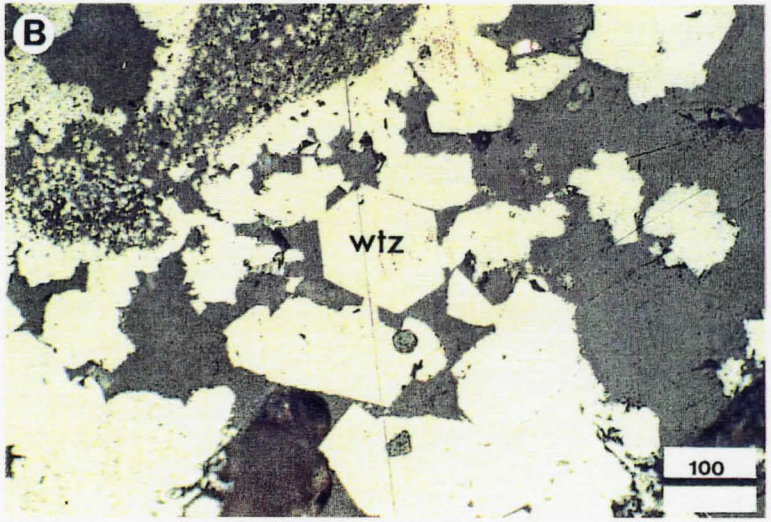
B
wtz
100

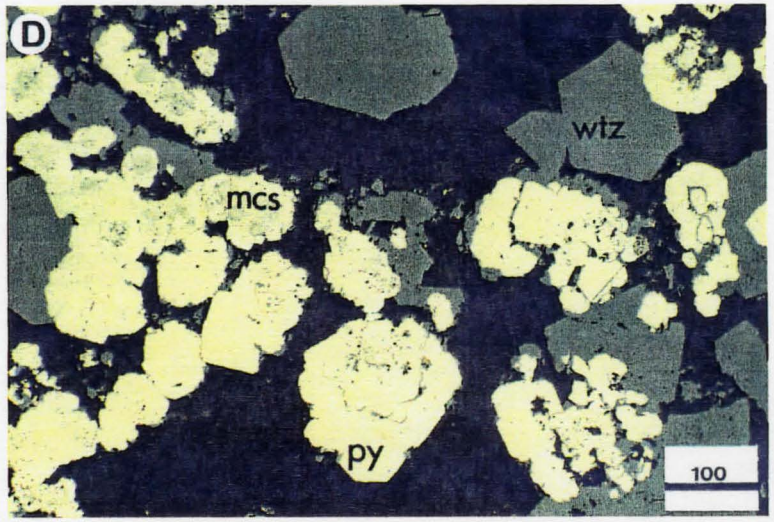
D
wtz
mcs
py
100

3.1.2 Sample XL1720-2B

Section XL-2B is cut from sample XL1720-2B. Textures in this sample are very similar to those in the previously discussed sections. Colloform growth patterns of Zn sulphide and Fe sulphide again occur as concentrically banded colloforms, occupying a large percentage of the total volume in this sample. Intergrown framboidal marcasite and colloform sphalerite are commonly found in association in other similar seafloor massive sulphides (Picot and Fevrier 1980; Oudin 1981,1983a; Kingston et al. 1983; Koski et al. 1982; Koski et al. 1984; Hekinian and Fouquet 1985). As in sample XL1720-2A, rings formed by alternating growth bands of the two phases are common. Granular aggregates of pyrite often display excellent growth rings with thin veneers of sphalerite seperating major periods of Fe sulphide growth. This textural feature is particularly spectacular in this sample.

Also found in these zones of open space deposition are very euhedral crystals of wurzite which sometimes reach 250 microns in diameter (Fig.3.3d). The largest of these crystals are strongly pitted (Fig.3.4a), which likely has resulted from preparation of the section however, the instability of wurtzite which results in dissolution might also be the cause. Many smaller crystals of wurzite and sphalerite are distinguishable under transmitted light. The largest sphalerite grains lie in one small area of the section, and

FIGURE 3.4. Photomicrographs emphasizing textural features found in sample XL1720-2B (A,B), and in Scott's Pinnacle (C,D). Scale bars are in micrometers. A) Pitted wurtzite crystals and sphalerite aggregates. B) Dendritic growth forms of Zn and Fe sulphides. C) Clusters of granular sphalerite. D) Granular pyrite and sphalerite with some weakly developed dendrites.

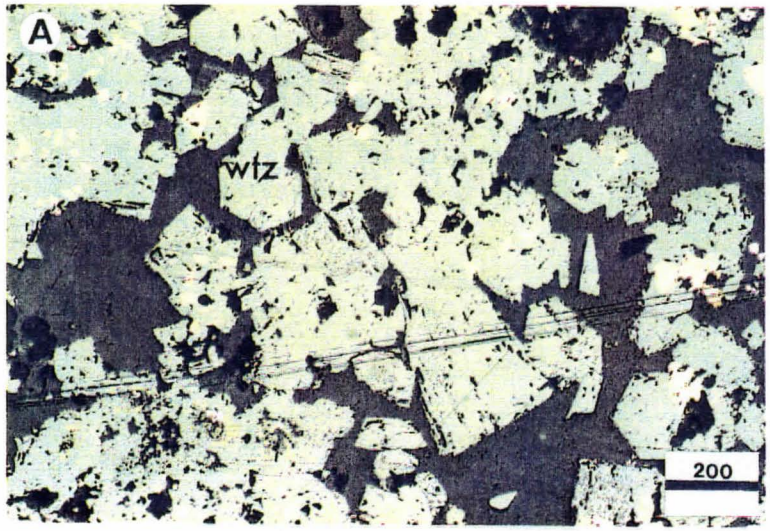
A
wtz
200

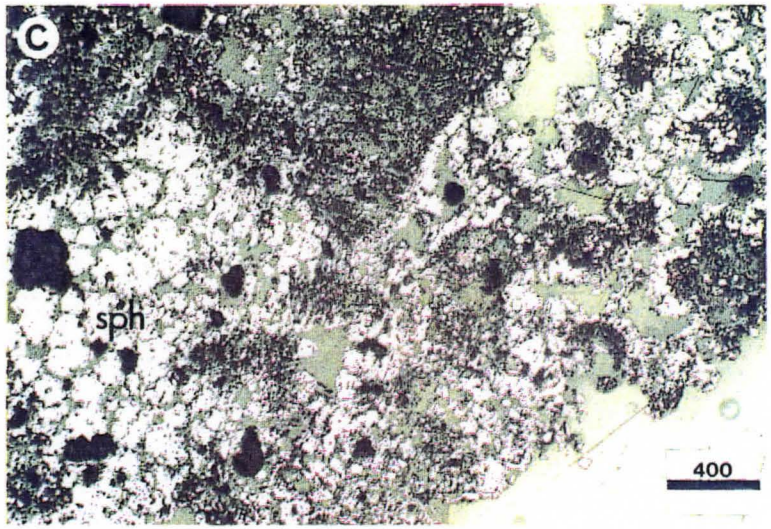
C
sph
400

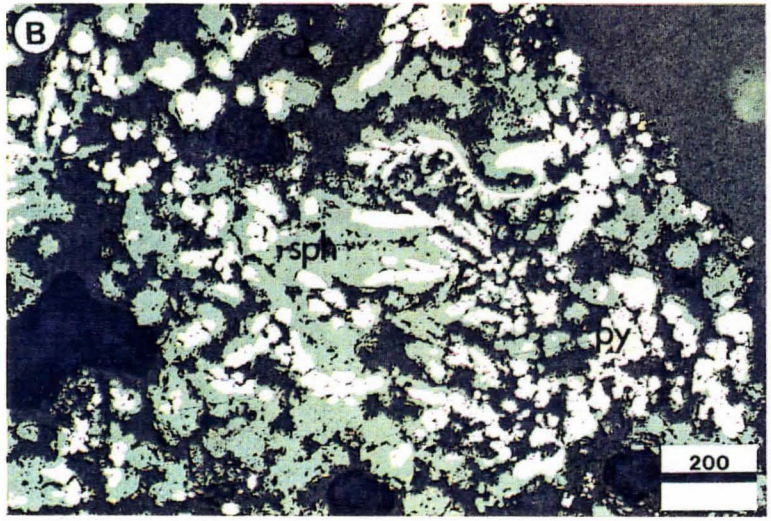
B
rsph
py
200


D
py
sph
400

some transmit light quite well. Because of this, they are the most likely source for workable fluid inclusions. A similar zone was described for the previous section (XL-2A2). Dendrites of Zn sulphide and Fe sulphide are rare in this section but, where they occur they are distinctively elongate (Fig.3.4b).

Overall the section shows a weakly developed large-scale layering; however, the areas of coarse wurzite have relatively sharp borders with wide zones of coarse sphalerite aggregates. A number of the large sphalerite grains continue to exibit textures indicative of "chalcopyrite disease", as rows of Cu-Fe sulphide blebs are totally emersed in sphalerite. Chalcopyrite is also dispersed as clusters of small grains set in a network of coarse grained sphalerite.

Silicates and sulphates constitute only a very small proportion of the total mineralogy, with textures similar to those described in the earlier sections.

3.1.3 Scott's Pinnacle

Section XL-3A is cut from a small sample taken from Scott's Spire whose location was given earlier. The sample itself comes from a portion of the spires outermost wall. Obviously, one polished section cannot be completely representative of the complex mineralogical variations that exist within the spire. A detailed description of the spire

is given by Hannington and Scott (1988). The mineralogy and paragenesis of the Axial Seamount spire is typical of that for white smoker chimneys at 21^{0}N (Oudin 1981,1983a; Haymon and Kastner 1981; Hannington and Scott 1988). In general, most of the precipitates in this sample are fine grained. Early low-temperature barite-silica deposition constructs the framework on which the later high-temperature, main sulphide stage will build. Delicate silica threads produced by bacteria are nicely preserved. This feature is documented in other Axial Seamount samples as well (Juniper and Fouquet 1988). Large amounts of very fine-grained barite and silica occur throughout the section, with a considerable proportion of the total volume remaining as open pores. Small amounts of anhydrite are also present.

The main stage of sulphide deposition is well represented by more coarsely grained aggregates of anhedral sphalerite (Fig.3.4c). A narrow zone of pyrite, which constitutes the bulk of the Fe sulphides in the section, borders the main zone of sphalerite. Well developed colloform pyrite and sphalerite form a wide band that runs through the section. This likely represents a portion of the second stage, in the main-stage period of sulphide deposition (Hannington and Scott 1988). Bordering the massive zones of colloform textured sulphides are dendrites consisting of sphalerite, pyrite and small amounts of framboidal marcasite (Fig.3.4d).

Smaller amounts of pyrite and early marcasite are distributed throughout the section as disseminated spheroidal aggregates set amongst the early amourphous silica (Hannington and Scott 1988). Wurtzite is not visible in this section, a likely result of its usual confinement to the interior of such deposits (Haymon and Kastner 1981; Oudin 1981, 1983a, Koski et al. 1984).

Tiny grains of chalcopyrite are found, often in clusters, within the larger grains of sphalerite, and are likely of replacement origin (ie. "chalcopyrite disease"). The minor and trace sulphide phases such as galena and jordanite were not observed in this section.

One problem of note concerning polished sections cut from sulphide samples originating from Axial Seamount and other similar deposits is that sometimes the surface is quite heavily pitted, owing to the extreme friability of the material.

3.2 Middle Valley

Sulphide samples from Middle Valley include dredge numbers MVDR02-01, MVDR02-05, and MVDR06-03 with respective polished thin section numbers MV-DR1, MV-DR2, AND MV-DR3. These sections are described in one discussion which involves periodic referrals to each of the three samples. The fine-grained nature of the precipitates along with their opacity,

has unfortunately, not permitted fluid inclusion analysis, and for this reason a combined and condensed description of these samples is presented.

The most abundant sulphide mineral is pyrrhotite which commonly occurs in open interlocking networks of tabular plates. These plates are often greater than 1 mm in length. The best examples are found in section MV-DR3 where pyrrhotite is abundant (Fig.3.5a,b). Many of the pyrrhotite laths have thin rims of pyrite and occasionally are infilled by Fe-rich sphalerite, a texture common to the Middle Valley sulphides described by Goodfellow and Blaise (1988). Open cavities in section MV-DR1 contain similar pyrrhotite. These cavities are partially surrounded by thin bands of subhedral Fe and Zn sulphides (Fig.3.5c), which use the skeletal network of pyrrhotite as a substrate for encrustation (Davis et al. 1987). In section MV-DR2, pyrrhotite is extensively replaced by pyrite and marcasite, which pseudomorph the grains they are replacing (Fig.3.6a). This texture has previously been described as "lacy" (Goodfellow and Blaise 1988). Well-developed framboids of marcasite also occur in this section.

Large areas of section MV-DR1 are occupied by colloform Fe and Zn sulphides that have clearly developed growth rings (Fig.3.6b). Fe sulphides comprise the bulk of these structures. Massive granular aggregates of sphalerite also form a large percentage of the total sulphide volume in

FIGURE 3.5. Photomicrographs of textures typical to Middle Valley sulphide samples. Scale bars are in micrometers. A) Large tablets of pyrrhotite with thin veneers of pyrite and Zn sulphides (MV-DR3). B) Heavily replaced laths of pyrrhotite with neighbouring sphalerite and Cu-Fe sulphides (MV-DR3). C) Fe and Zn sulphides encrusting a network of skeletal pyrrhotite (MV-DR1).


A
po
200

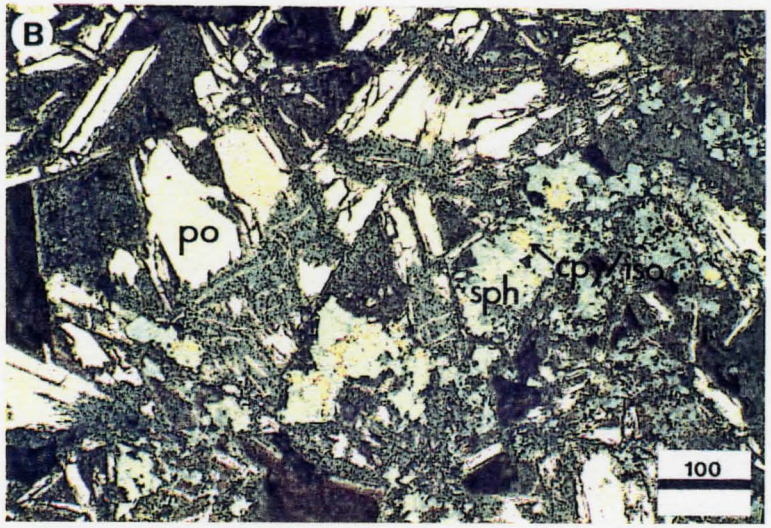
B
po
sph
cpy/isa
100

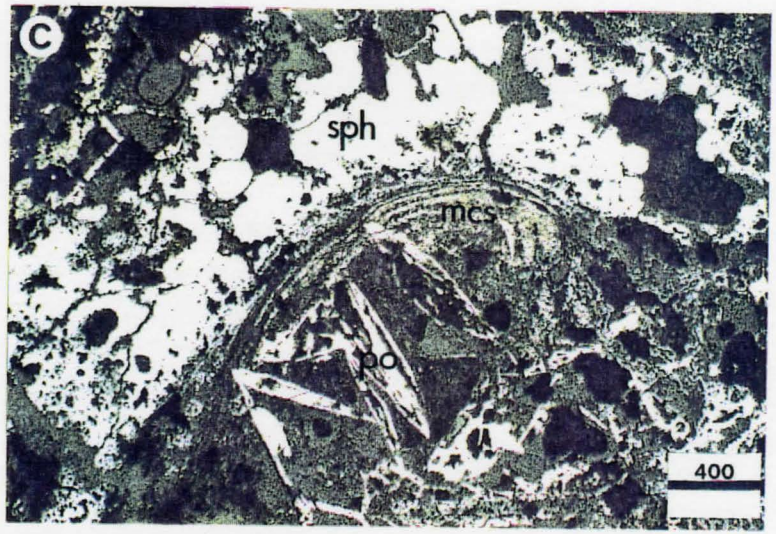
C
sph
mcs
po
400

FIGURE 3.6. Photomicrographs of textures displayed by Middle Valley sulphide samples. Scale bars are in micrometres. A) Framboids of marcasite and pyrite replacing pyrrhotite (MV-DR2). B) Colloform Fe and Zn sulphides with multiple growth bands (MV-DR1). B) Lamellae of a possible oxide mineral (white) included within sphalerite (MV-DR1).

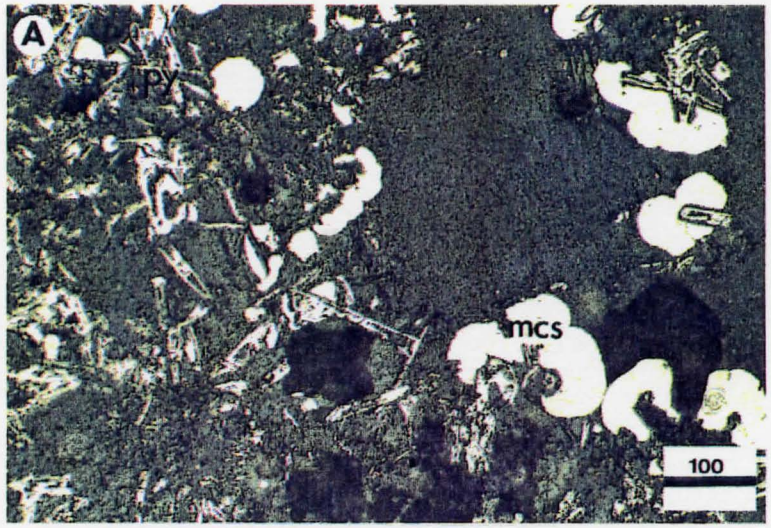
A
py
mcs
100

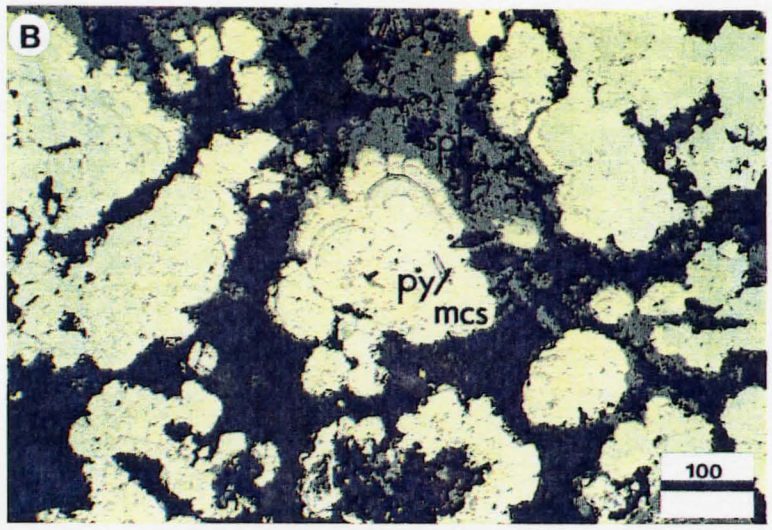
B
sph
py/
mcs
100

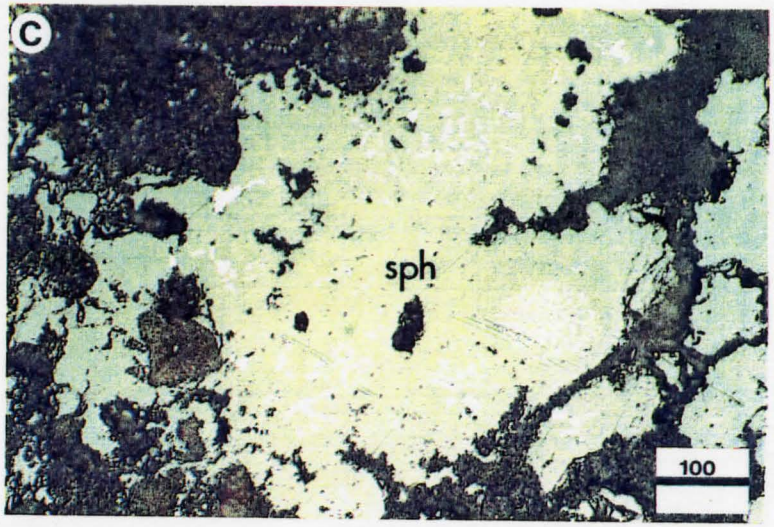
C
sph
100

section MV-DR1. Partial hexagonal outlines of some Zn sulphide grains indicates the inversion of wurtzite to sphalerite.

Cu-Fe sulphides are distributed within sphalerite in sections MV-DR1 and MV-DR3, but are virtually nonexistent in section MV-DR2. Chalcopyrite occurs as exsolution lamellae in isocubanite and as replacement rims around the edges. Several aggregates of sphalerite in section MV-DR1 contain small mamellar inclusions of an isotropic, white-coloured mineral that occurs, most distintively, as radial, spherical clusters (Fig.3.6c). The minerals hematite and magnetite in these samples, are known to result from the oxidation of Fe sulphides (Goodfellow and Blaise 1988). It may be, that Fe sulphides within the sphalerite aggregates, were oxidized. Galena is present in small amounts also and it is possible that Pb sulphide and and Zn sulphide were coprecipitating together.

Barite is intergrown with pyrite and silica but also occurs as subhedral grains set within the interstices of large sulphide clasts. Barite can also be found in fine rosettes distributed throughout the matrix of hemipelagic sediment where it is believed to be an alteration product of this sediment (Goodfellow and Blaise 1988). Talc is a common Mg silicate in these deposits and it occurs regularly as fibrous masses in association with barite. Amorphous

silica is dispersed throughout each section where it infills small pores and occurs within grain interstices.

CHAPTER 4

FLUID INCLUSIONS

4.1 Introduction

Fluid inclusions trapped during the formation of seafloor polymetallic sulphides offer an opportunity to determine the characteristics of fluids from which these deposits were formed. Not only have these inclusions escaped undeterminable tectonic processes such as those affecting many older deposits, but they also allow for very thorough investigation of the hydrothermal vent fluids as a result of their size which is often large (>50 microns).

Wurtzite, sphalerite, barite and amourphous silica have all been found to contain at least some inclusions. Data obtained from fluid inclusions in wurtzite has been documented by others in previous studies as mentioned in chapter 1. Homogenization temperatures for fluid inclusions in amourphous silica could not be obtained and fluid inclusions in sphalerite and barite have not been previously described.

Freezing and heating experiments were performed on suitable inclusions to obtain freezing point depression and homogenization temperatures respectively. Inevitably, a number of problems arose due to various effects related to both the physical nature of the samples as well as the operation of the

heating-freezing equipment itself. These problems are discussed, relating each to its effects on the measuring procedure. A physical description of the various inclusion types encountered during the course of this study follows below.

4.2 Fluid Inclusion Descriptions

4.2.1 General

Fluid inclusions were located in the minerals wurzite, sphalerite, amorphous silica, and barite. Unfortunately all of the sections prepared for this study do not contain measureable inclusions and only one sample (XL1720-2A) contains measureable inclusions in more than one mineral phase.

The sections from Middle Valley samples MVDR02-01, MVDR02-05, and MVDR06-03 were scanned visually many times for inclusions but, only a few very minute inclusions (<1 micron) could be located. In general, more than 90 % of the section, in each case, is simply too opaque for positive identification of useful inclusions. The overall opacity of these sections is a result of difficulties encountered during the preparation procedure which is made difficult by the very friable nature of the samples. Sections are polished to a manageable thickness at which time they are impregnated in a high-temperature epoxy. The sections are then doubly

polished and are taken down to a thickness between 50 and 100 microns. Acetone was used to dissolve the epoxy and free the thin section from the microscope glass. The delicate sections were moved onto microscope cover slips which were placed carefully within the heating/freezing stage for measuement. Thicknesses not less than approximately 150 microns were achieved for these sections, a result of the delicate physical nature of the samples. A thickness of about 100 microns is best suited for fluid inclusion work.

The high content of fine-grained hemipelagic sediment in the Middle Valley samples also contributes to obscure visual clarity in the polished thin sections.

The Axial Seamount samples also contained many fluid inclusions that were too small for acurate measurement (<5 microns) and many that were too small to make the vapour phase discernable (<1 micron). However, these samples were far superior to those from the Middle Valley location. Many fluid inclusions were located in samples XL1720-2A and XL1720-2B, a number of which proved to be useful for freezing and heating experiments.

By far, the bulk of the measureable inclusions were found in the largest grains of sphalerite, even though greater than 99 % of all the inclusions in sphalerite are far to small for measurment purposes. A variety of inclusion forms are present in sphalerite and each will be described in

the following section.

4.2.2 Inclusion Classification

Inclusions can be grouped into three main types with a fourth type representing solid inclusions.

Type A inclusions: These inclusions are best described as large complex fluid inclusions expanding upwards from growth surfaces, often consisting of a maze of multiple interconnecting arms and tails (Plate 4.1).

The range in size of these inclusions is difficult to determine due to their complexity, especially when considering the lower limit. The upper size limit is no less than 100 microns lengthwise with the largest extending into regions which were not optically traceable (ie. opaque areas in the sphalerite grains) (see Plate 4.1). Often the complicated growth forms assumed by such inclusions contain a few unconnected portions which have an identifiable vapour phase. The vapour phase in the larger networks is usually not discernable, as almost all of these inclusions have a similar appearance to inclusions that have necked-down.

These inclusions may represent healed fractures which originally resulted during crystallization and hence they could be described as pseudosecondary; however, most are probably only exaggerated examples of growth inclusions. If

Plate 4.1. Photomicrographs of large, complex two-phase fluid inclusions on growth surfaces in sphalerite. Scale bars are in micrometres. Photomicrographs are taken at equal scales. A and B (XL-2A2) are examples of type A inclusions.

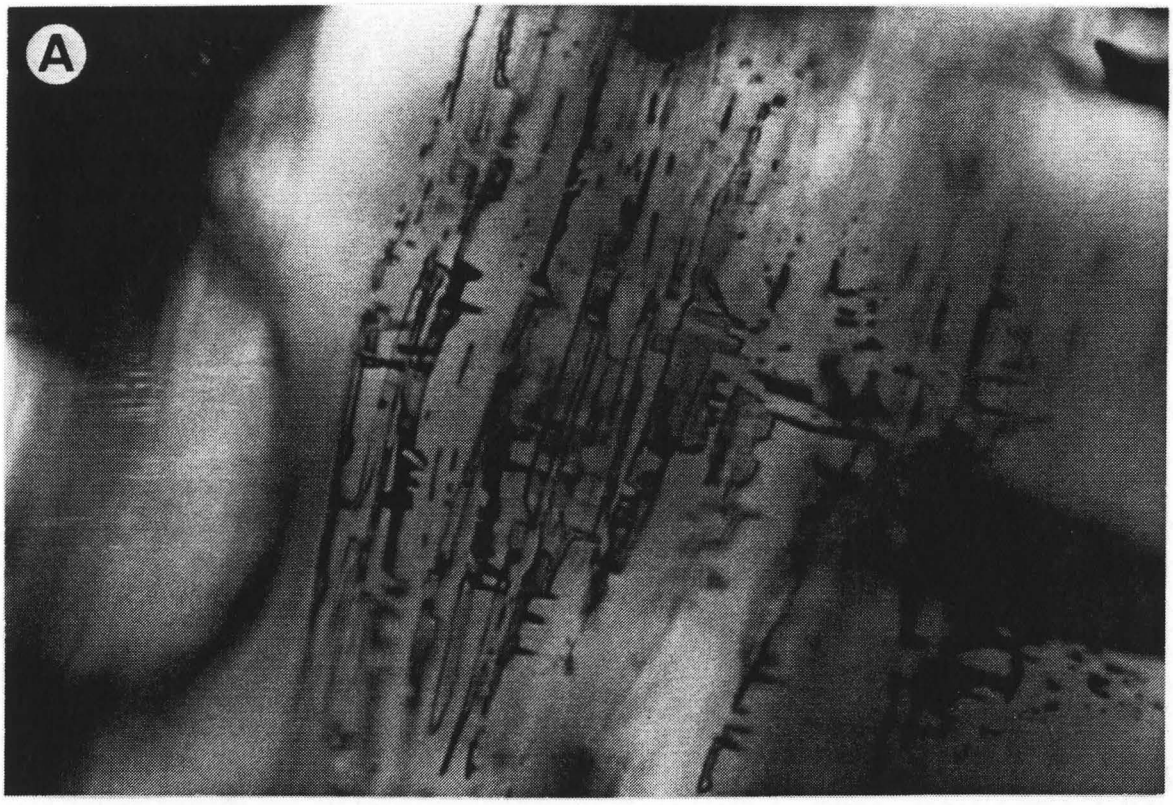
A

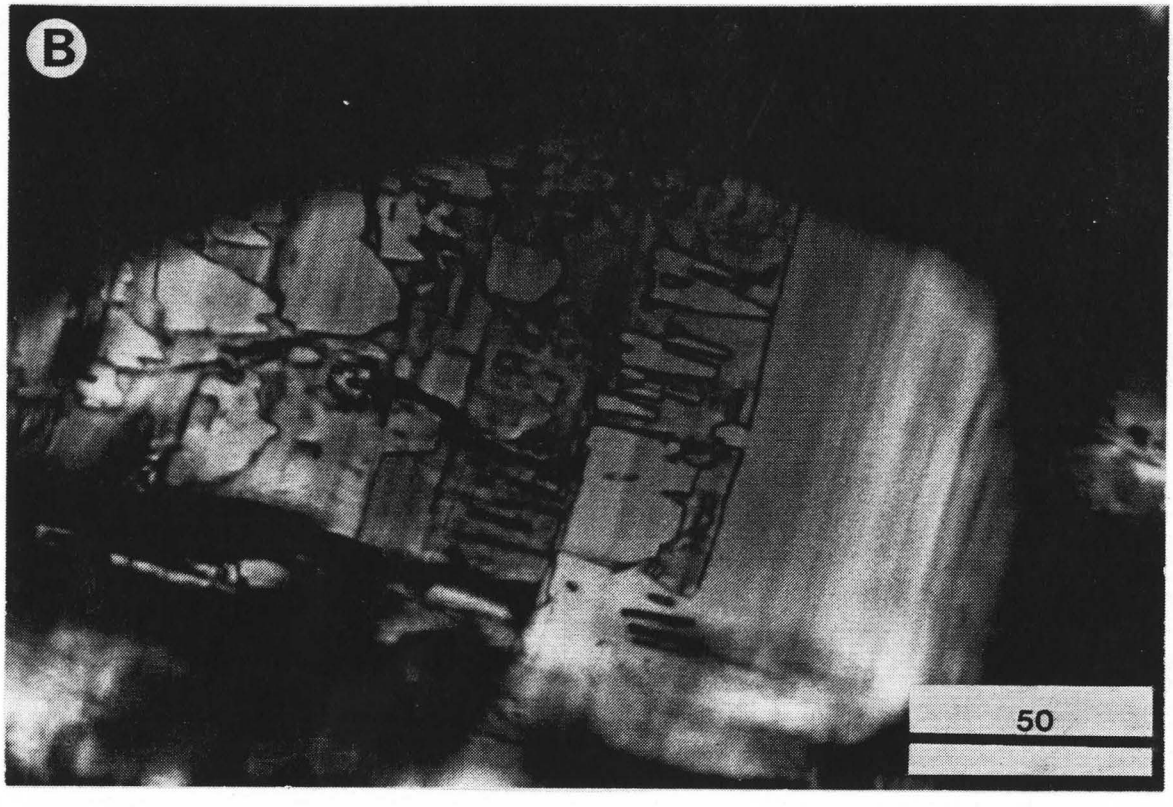
B
50

a sufficient nutrient solution is unavailable, starvation may occur and crystal growth may be sporadic. Hence, the crystal tends to trap a series of very large inclusions, flattened parallel to a crystal face, with only thin septa of crystal seperating each chamber (Roedder 1984). The possibility that these inclusions have leaked or that they are pseudosecondary definitely exists and hence, none of these inclusions were suitable for measurement.

Type B inclusions: These inclusions, are in effect, the main subset of type A inclusions. They occur as rows or clusters spread along growth surfaces or twin planes and are usually somewhat elongate with at least one flat wall surface in most cases, representing the surface of the inclusion against a smooth crystal surface (Plate 4.2).

Sizes of type B inclusions range from << 1 micron to 30 or 40 microns. Many are extremely long and narrow or almost tubular in shape. Type B inclusions are often arranged in groups according to increasing or decreasing size (Plate 4.2a,d,e). Some display irregular shapes which are the result of increased or decreased periods of crystal growth. The largest of these inclusions are the most useful for measurement purposes since they clearly show both a liquid and a vapour phase (see Plate 4.2b,c,d). Growth inclusions

PLATE 4.2. Photomicrographs of two-phase fluid inclusions in sphalerite. Scale bars are in micrometres. Photographs A,B and C (XL-2A2), and D and E (XL-2B) are at the same scale and represent examples of type B inclusions.

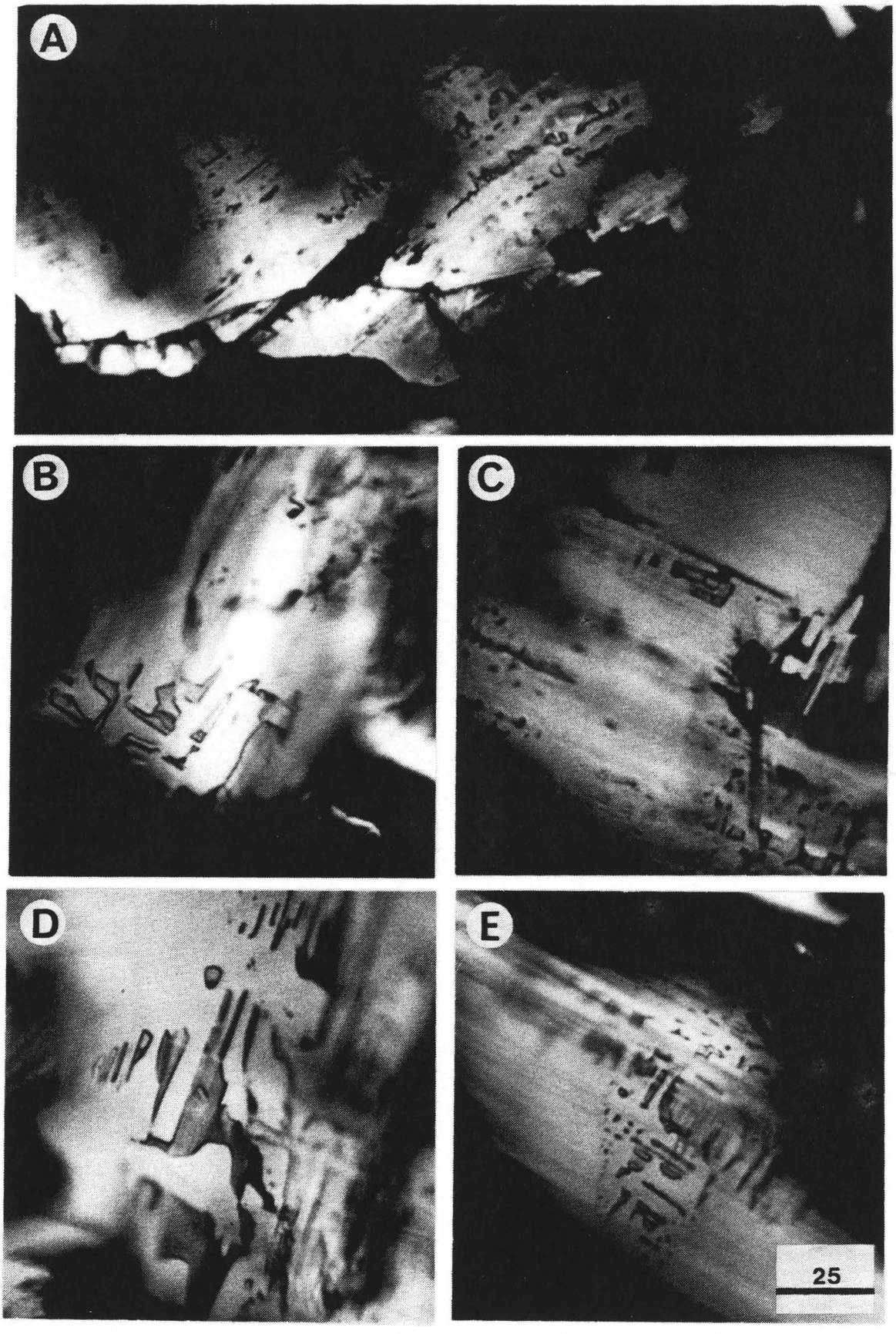
A
B
C
D
E
25

are described by Roedder (1984) and by Shepherd et al. (1985).

Type C inclusions: Type C inclusions are rounded to subrounded, are less elongate than types A or B inclusions, and are situated well away from most other inclusions.

These inclusions are typically 1 to 10 microns in length. Those that are greater than 5 um have a reasonably well defined vapour phase, some of which were adequate for analysis. The isolation of these inclusions from large groups of inclusions is likely the result of a small flaw or perturbation such as a surface crack on an otherwise smooth crystal surface, which acted as a point of cohesion leading to the trapping of fluid (See Plate 4.3). In a few instances, type C inclusions were found in pairs as well.

Type D inclusions: These are solid inclusions that assume a number of different forms, the most common being large flat plates and tiny flecks of varied sizes.

These inclusions are noted for reference sake and because large numbers of solid inclusions are visible in all of the sections, sometimes obscuring the view to useful fluid inclusions. The larger plate-like solid inclusions are common to sphalerite whereas smaller flecks are widespread in tabular crystals of barite. The solids are likely fine precipitates of sulphides although no positive identification

PLATE 4.3. Photomicrographs of two-phase fluid inclusions in sphalerite. Scale bar in micrometers. Photomicrographs A,B,D,E, and F (XL-2A2), and C (XL-2B) are at the same scale and represent examples of type C inclusions.

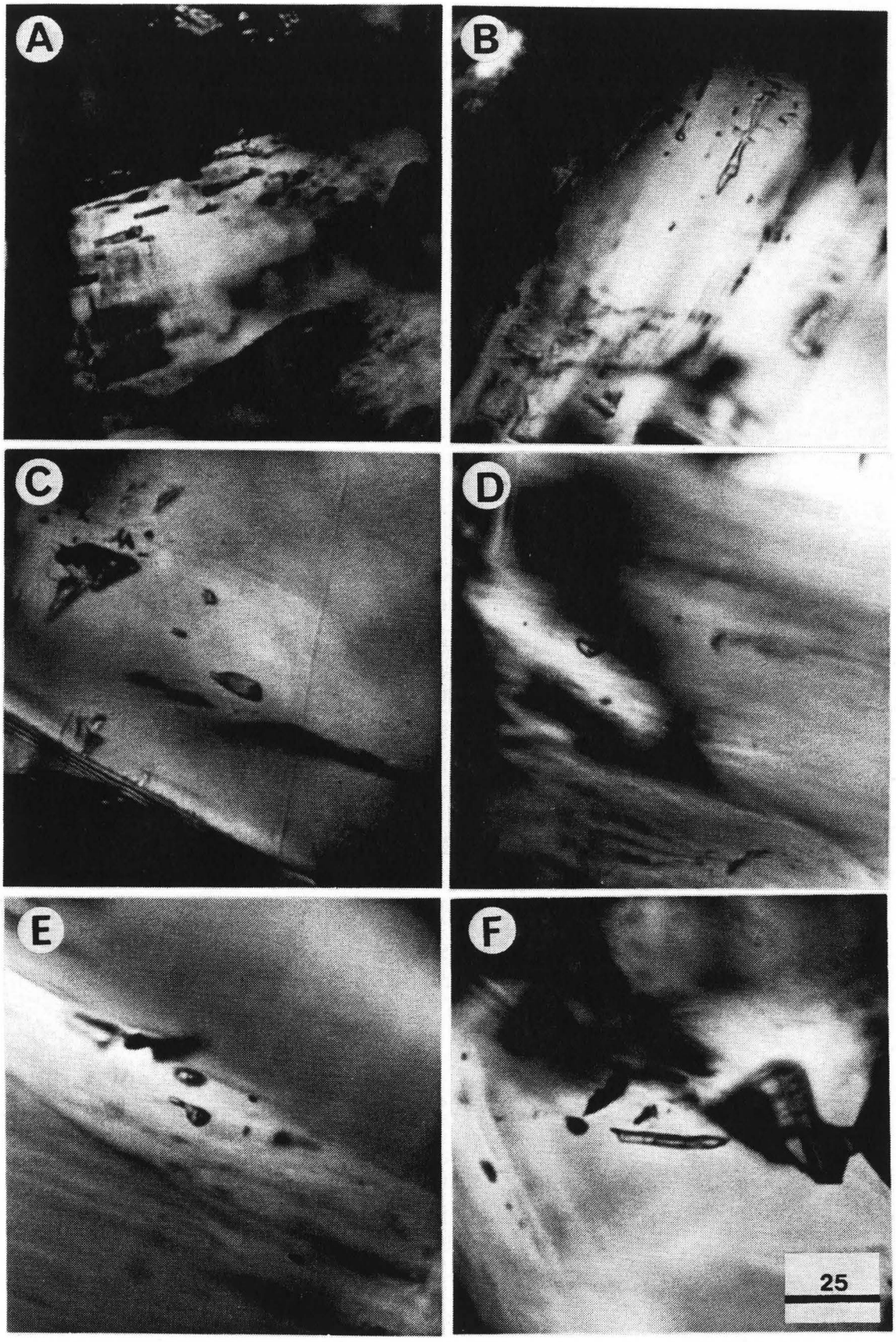
A
B
C
D
E
F
25

was made.

The fluid inclusions types just described, represent a very generalized classification and the groupings could easily be subdivided into further subgroups, or classified according to different criteria. For the purpose of this study however, a simple classification is desirable, especially in light of the actual numbers of workable inclusions and their limited host minerals.

Other than sphalerite, fluid inclusions found in amourphous silica and barite are primarily growth inclusions. These inclusions have relatively simple morphologies, with the bulk having elongate forms with rounded ends. Elongate inclusions were found aligned opposite to one another along growth surfaces within amourphous silica. A few were discovered with irregular shapes, such as those lying between crystal boundaries as in barite rosettes. The relative abundance of inclusions greater than 5 microns in size, as compared to inclusions in sphalerite, was much smaller. The few that were large enough for measurements could be found in sections XL-2A1-A and XL-2A1-B, from Axial Seamount sample XL1720-2A.

4.2.3 Basic System

Freezing studies are the most useful means of determining the salinity of aqueous inclusions since the

depression of the freezing point of pure water is directly proportional to the amount of salt in solution (Fig.4.1a). By reheating a frozen inclusion and determining the temperature of final ice melting (T_M) we can estimate the amounts of dissolved salts. It is known however, that T_M varies in accordance with the composition of the solution, and differs slightly depending on which of the various chloride salts are present (Fig.4.1a). Due to the complexities involved in determining fluid composition, T_M, when used to calculate weight % salts, will be expressed as equivalent to NaCl content alone. Even if the solution were a Ca-Na-K-Mg chloride mixture, it is generally assumed that the error resulting from estimates based on an NaCl equivalent solution is < 5% (Clynne and Potter 1977; Shepherd et al. 1985).

During heating tests on liquid plus vapour inclusions, the vapour phase will homogenize to the liquid phase by shrinkage and eventual disappearance. NaCl in solution, like most other salts, raises the critical point of the mixture (Fig.4.1b). This is of interest when considering weight percent salt contributions to the homoginization temperatures of two-phase fluid inclusions. Significant increases in temperature of homogenization result in unsaturated aqueous sodium chloride solutions with a change of only a few weight % salt. It is important to keep this in mind when reviewing experimental results from fluid inclusion measurements as it

FIGURE 4.1a. Depression of the freezing point of pure water as a function of weight percent salt in solution for selected chloride salts (from Shepherd et al. 1985).

FIGURE 4.1b. Position of the liquid-vapour curve and slope of compositional isochores within the liquid field of the H_2O-NaCl system, as a function of salinity (from Shepherd et al. 1985). Labels for isochores are in gcm^{-3}. Points A and B represent sample compositions at a given pressure (900 bars). Other labels are: L = Liquid field, V = Vapour field, T_T = Trapping temperature, T_H = Homogenization temperature.

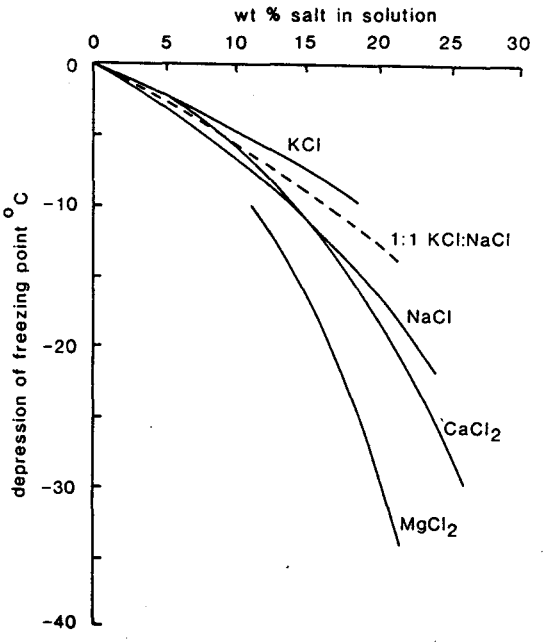
wt % salt in solution
0
5
10
15
20
25
30
0
-10
-20
-30
-40
depression of freezing point °C
KCl
1:1 KCl:NaCl
NaCl
CaCl2
MgCl2

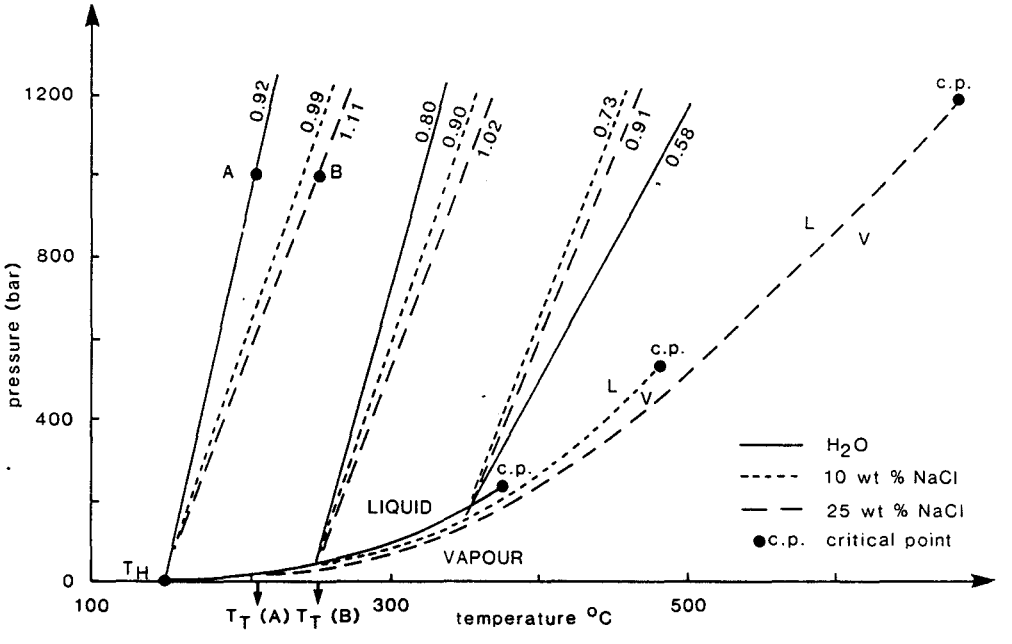
1200
800
400
0
pressure (bar)
0.92
0.99
1.11
0.80
0.90
1.02
0.73
0.91
0.58
A
B
c.p.
c.p.
c.p.
L
V
L
V
LIQUID
VAPOUR
TH
TT (A)
TT (B)
100
300
500
temperature °C
H2O
10 wt % NaCl
25 wt % NaCl
c.p. critical point

often provides a simple explanation of wide ranges in recorded temperatures.

Experimental results of heating and freezing experiments and some of the implications will be discussed in section 4.4.

4.3 Analytical Equipment

4.3.1 Fluid Inclusion Apparatus

The apparatus utilized for measuring fluid inclusions in this study was the adapted U.S.G.S. gas-flow heating/freezing system made by FLUID INC. of Denver Colorado. Please refer to Plate 4.4 for the various equipment mentioned in the following discussion.

The system includes a Nikon Optiphot binocular microscope, equipped for fluid inclusion studies, and a heating/freezing stage which utilizes nitrogen vapour distilled off liquid nitrogen for cooling and hot air for heating. The heating/freezing stage is entirely enclosed and insulated. A temperature sensitive thermocouple runs into the stage and the wire tip is set, such that it touches the sample and records the temperature accurately. The temperature can be read from the digital display on the calibrated trendicator. Fine temperature control is achieved by using the variac which is itself connected to a wire torch set within the heating/freezing stage. The small gas valves on

PLATE 4.4. Fluid inclusion apparatus utilized in this study. Metre stick on bench provided for scale (cm and inches). 1.) JVC High Band Saticom Colour Camera. 2.) JVC Colour Video Monitor. 3.) Nikon Optiphot Binocular Microscope 4.) Trendicator digital temperature readout panel. 5.) Gas-flow valves for fine adjustment of temperature. 6.) Temperature variac. 7.) Thermocouple mount. 8.) Heating/freezing stage 9.) Wire to electric heating torch. 10.) Liquid nitrogen flow valves and hose. 11.) Liquid nitrogen dewar 12.) Gas lines to microscope stage, trendicator, and liquid nitogen dewar. 13.) Gas regulators. 14.) Gas tanks. 15.) Wire to foot control for temperature variac.

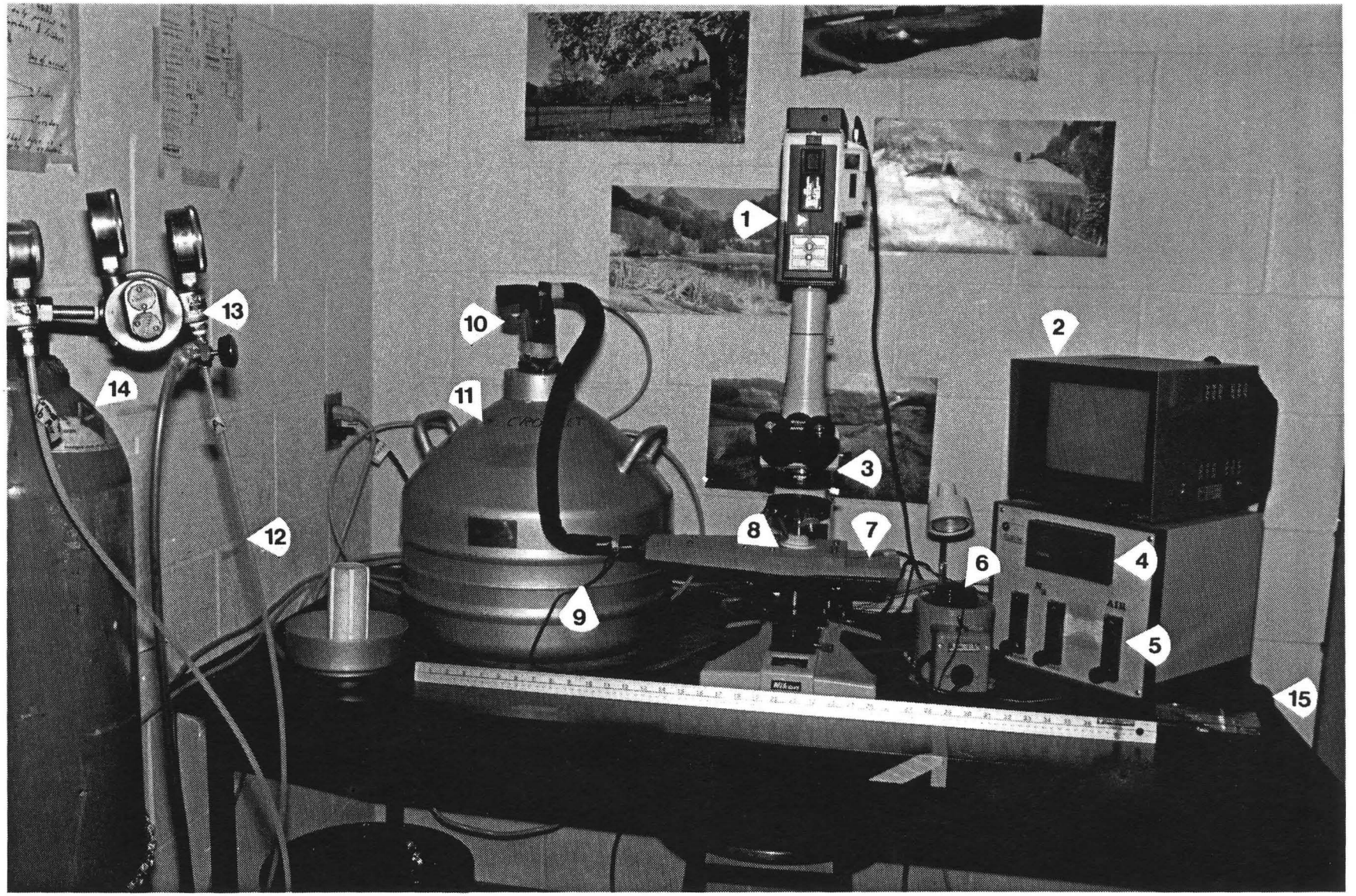
1
2
3
4
5
6
7
8
9
10
11
12
13
14
15

the trendicator can also be used to help control the temperature. By careful manipulation the temperature can be maintained to within 1^0 C/min.

Also available for this study was a JVC TM-90CA, 7 inch, Colour Video Monitor with 800 lines resolution, connected to a JVC GX-S700 High Band Saticom Colour Camera, set onto a DIAG 5000 microscope adapter.

Complete details for the set-up and operation of the gas-flow heating/freezing system can be found in the document: FLUID INC. adapted U.S.G.S. GAS-FLOW HEATING/FREEZING SYSTEM, INTRUCTION MANUAL.

4.3.2 Photomicrography

Microphotographs of fluid inclusions (See pages 40,42, and 44, Chapt.4, Section 4.3) were taken with a Nikon Microflex automated system, with 30 % integrated measurement and an FX-35 manual advance dark box. The dark box is mounted to a 35mm camera adapter and the adapter is mounted to the Microflex main body. This assembly fits into the phototube of the Nikon microscope. The highly sensitive silicon photodiode light detector responds to even very low levels of light, making it possible to obtain good results when photographing inclusions in dark minerals such as sphalerite.

All fluid inclusion microphotography was performed using Kodak 3200 speed, black and white film, with ASA set to 1600.

Reflected light photography (See chapt.3) was completed using a standard 35 mm Leitz camera back, mounted onto a Leitz Metalloplan binocular microscope.

4.4 Method and Results

4.4.1 Calibration

Before attempting freezing and heating measurements, those components of the FLUID INC. gas-flow heating/freezing system essential for temperature calibration must be recalibrated. The DORIC model 410A trendicator is calibrated by measuring the thermocouple response against several known calibration standards. The trendicator is calibrated for three temperatures which cover the working range of temperatures required throughout the course of the study. Calibrations were made at the freezing temperature of pure, triple distilled mercury ($-39.4^{0}C$), at the freezing point of pure distilled water ($0.0^{0}C$), and at the freezing point of the compound sodium nitrate ($+306.8^{0}C$). This range of temperatures is expected to cover those encountered during observations of fluid inclusion behaviour for the seafloor sulphide samples.

The equipment was calibrated prior to commencing freezing and heating experiments on fluid inclusions and once again towards the end of the study when the thermocouple deteriorated and required replacement.

Results obtained from heating and freezing inclusions in sphalerite, are discussed in the following sections.

4.4.2 Procedure and Results: Freezing Experiments

Measurements of the freezing point depression of fluid inclusions have been determined to calculate the weight % salts in solution. The system H_2O-NaCl can be complex, depending on the amount of salts contained within the fluid, even when an NaCl equivalent composition is assumed. Several points must be made before discussing the results.

Three solid phases may crystallize in the H_2O-NaCl system: ice, hydrohalite ($NaCl*2H_2O$), and Halite (NaCl). Two phase changes must be considered including, the first appearance of liquid during a warm-up cycle after complete freezing, and the melting of salt hydrates. The first appearance of liquid, or the temperature of first melting T_{fm}, corresponds to the eutectic temperature, -20.8^0C (Fig 4.2). Where solid solution between the solid phases does not occur, eutectics are invariant points which allow melting to occur at a temperature determined by the end member composition alone (Hollister and Crawford 1981; Roedder 1984; Shepherd et al. 1985).

Initial melting observations indicate that the salt content of the Juan de Fuca inclusions will be less than the salt content required for a eutectic composition, 23.3 weight

% ; however, the final ice melting temperature should not be used alone to determine the composition of the fluid because a similar range of final melting temperatures occurs between 0 weight % NaCl and the eutectic composition, and the eutectic composition and 26.3 weight % NaCl. At salinities above 26.3 weight % NaCl, $NaCl*H_2O$ melts incongruently to NaCl and solution. For compositions lying between the eutectic and 26.3 weight % NaCl, the solid phase hydrohalite should be recognized, whereas ice is the only solid phase at salinities less than the eutectic (Fig.4.2)..

During the course of experimentation, observations of individual ice crystals formed upon reheating of a frozen inclusion were made extremely difficult by the physical nature of the inclusions and the deep coppery colour of sphalerite. Differentiation of ice crystals from hydrohalite crystals was made practically impossible.

Freezing of less saline solutions is accompanied by a notable shrinkage in the volume of the vapour bubble (Hollister and Crawford 1981). Vapour bubble contraction was in fact one of the most pronounced changes observed in freezing these inclusions. Also, high relief between the solid phase and the solution was not observed, indicating the probable existence of ice only, as opposed to hydrohalite. If the latter phase was present, then individual crystals would probably have been more easily recognizable since contrast

FIGURE 4.2. Temperature-composition phase diagram for the system H_2O-NaCl showing low temperature phases in equilibrium with vapour (from Shepherd et al. 1985).

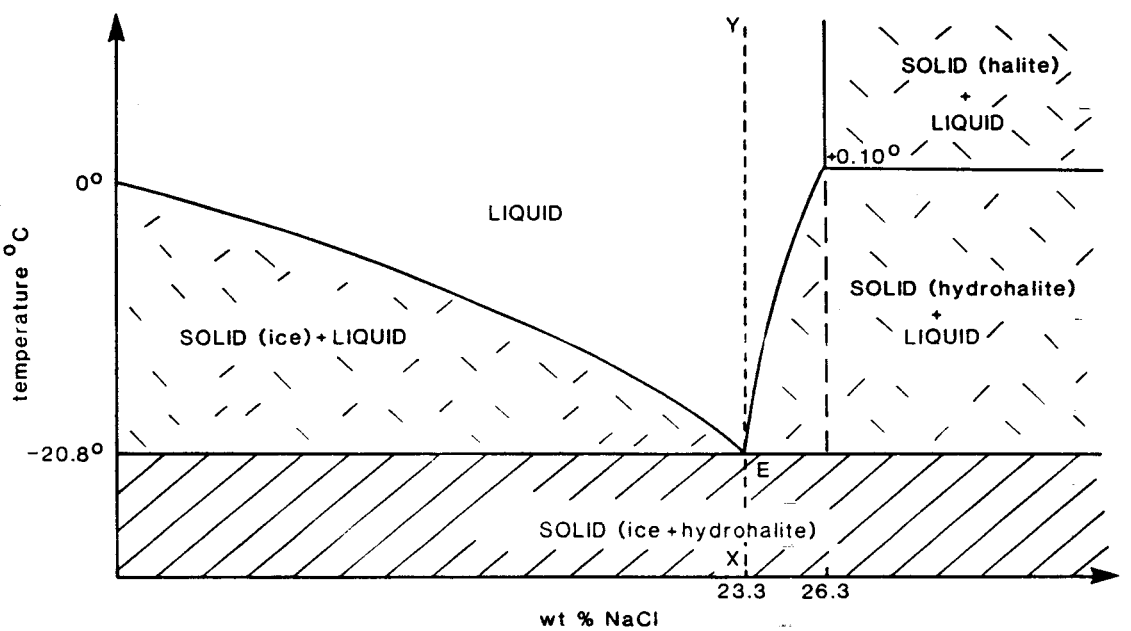
Y
SOLID (halite)
+
LIQUID
+0.10°
0°
LIQUID
SOLID (hydrohalite)
+
LIQUID
temperature °C
SOLID (ice) + LIQUID
-20.8°
E
SOLID (ice + hydrohalite)
X
23.3
26.3
wt % NaCl

differences and the index of refraction would be more pronounced.

Freezing point depression temperatures were determined by warming frozen inclusions gradually until ice crystals no longer regrow with removal of heat source (ie, critical point is reached). This temperature can be used to calculate weight % salts using a linear regression least squares method outlined by Potter et al. (1978) (Roedder 1984).

$W_S = 1.76958\phi - 0.042384\phi^2 + 0.00052778\phi^3$ (+/- 0.028 %)

Where W_S = Weight % salts

ϕ = Freezing point depression (^0C)

This equation is used since it allows for a simple determination of W_S by substituting the temperature representing freezing point depression.

An inclusion in section XL-2B (Spalerite grain #1, inclusion A) has a freezing point depression averaged to be -4.1^0C. Calculating for weight % NaCl we arrive at, W_S = 6.5792 +/- 0.028 %. Please see Tables 4.1 and 4.2 for a list of measured inclusions and calculated compositions.

Attempts were made to measure freezing point depression in inclusions in barite and amorphous silica; however, visual problems arising from the freezing and thawing process prevented accurate estimates of the freezing point depression. Slight contractions of the heating/freezing stage and/or the mineral itself meant that refocusing was necessary and hence

observations of discrete physical changes for these inclusions became futile.

In other samples from Axial Seamount, Chen et al. (1982) report low salinities, a condition necessary to achieve silica saturation and precipitation at ~235^{0}C, the homogenization temperature of the inclusion upon heating. This requires sufficient conductive cooling and mixing of a 350^{0}C end member hydrothermal fluid with ambient seawater near the site of deposition (Hannington and Scott 1988). Homogenization temperatures (see 4.4.3), show that the temperature for sphalerite deposition, from the present study, lies in the same range. As amorphous silica and sphalerite have been co-precipitated periodically, it leads one to assume that the salinities involved are representative of substantially diluted hydrothermal fluids. Composition of fluid inclusions may therefore, be determined safely using the temperature of final ice melting singly.

TABLE 4.1. Freezing temperature data for sample XL1720-2A, section XL-2A2. W_S = Weight % NaCl, ϕ = Freezing point depression, SD = Standard Deviation, SD_W = Standard deviation of weight % NaCl data, SD_ϕ = Standard deviation of freezing point depession values.

Grain #	Inclusion	ϕ (Avg.^{0}C)	SD_{ϕ}	W_S	SD_W
1	A	3.80	0.00	6.14	--
1	B	3.80	0.46	6.14	--
1 (Avg.)	-----	3.80	0.00	6.14	0.0
2	A	3.50	0.71	5.70	--
2	B	3.60	0.71	5.85	--
2 (Avg.)	-----	3.55	0.07	5.77	0.1
3	A	3.45	0.21	5.62	--
3	B	3.90	0.28	6.29	--
3	D	3.80	0.00	6.14	--
3	F	3.45	0.14	5.62	--
3 (Avg.)	-----	3.65	0.24	5.92	0.3
4	A	3.75	0.21	6.07	--
4	B	3.50	0.27	5.70	--
4	C	3.75	0.07	6.07	--
4 (Avg.)	-----	3.67	0.14	5.94	0.2
5	A	3.55	0.52	5.77	--
6	A	3.50	0.42	5.70	--
6	B	3.45	0.50	5.62	--
6 (Avg.)	-----	3.48	0.04	5.66	0.1
7	A	4.15	0.07	6.65	--
7	B	4.05	0.35	6.51	--
7 (Avg.)	-----	4.10	0.07	6.58	0.1
8	A	4.00	0.00	6.43	--
9	D	4.15	0.07	6.65	--
9	E	4.05	0.07	6.51	--
9	F	4.15	0.07	6.65	--
9 (Avg.)	-----	4.12	0.58	6.60	0.1
Sample (Avg.)	-----	3.79	0.26	6.08	0.4

Grain #	Inclusion	ϕ (Avg.^{0}C)	SD_ϕ	W_S	SD_W
1	A	4.10	0.14	6.56	--
4	A	4.40	0.00	7.01	--
5	A	3.50	0.00	5.70	--
5	B	3.90	0.10	6.29	--
5 (Avg.)	-----	3.70	0.28	5.99	0.2
6	A	3.90	0.14	6.29	--
7	A	3.80	0.14	6.14	--
8	A	3.90	0.28	6.29	--
Sample (Avg.)	-----	3.93	0.28	6.33	0.4

TABLE 4.2. Freezing temperature data for sample XL1720-2B, section XL-2B. W_S = Weight % NaCl, ϕ = Freezing point depression, SD = Standard deviation, SD_W = Standard deviation of weight % NaCl data, SD_ϕ = Standard deviation of freezing point depression data.

4.4.3 Procedure and Results: Heating Experiments

Homogenization temperatures for inclusions in sphalerite were measured subsequent to completion of the freezing trials. Polished sections were removed from glass mounts on microscope slides by dissolving the impregnator/mounting glue with acetone. Great care was required in transferring the delicate sections from the slides onto circular microscope plates which fit into the heating/freezing stage chamber, thus avoiding direct handling of the fragile rock slice.

The temperature of homogenization (T_h) (ie. homogenization of a two-phase liquid plus vapour assemblage to one liquid) is rarely equivalent to the trapping temperature (T_t). Homogenization temperatures are usually a minimum estimate of trapping temperatures, the difference arising from the trapping of fluid at pressures greater than one atmosphere. Pressure corrections must be made in accordance with their calculated salinities, to obtain a true estimate of the trapping temperatures.

The relationship between pressure, temperature and density can be illustrated by a three dimensional plot, or by a two dimensional P-T plot with isochores, or lines of constant density, representing the fluid density (Fig.4.1b). Compared with pure water, saline inclusions, such as those of the H_2O*NaCl system, have higher critical point temperatures and higher temperature liquid-vapour field boundaries for a

given pressure. The slope of the isochores also change with increasing fluid density, which results in greater temperature corrections (Fig.4.1b).

Potter (1977) has compiled volumetric data for aqueous sodium chloride and evaluated these data by a weighted least-squares regression method, to produce graphs of corrected temperature (dT) vs. T_h for aqueous NaCl solutions (Fig.4.3a,b). These graphs can be used to correct T_h using the known fluid compositions calculated earlier, and hydrostatic pressures estimated from depths provided by bathymetric surveys. Graphs representing 5 and 10 weight % NaCl solutions will provide reasonable estimates of T_t for the 5.6 to 7.0 weight % range determined for these fluid inclusions.

As an example, inclusion A in sphalerite grain 1, from section XL-2B, has a temperature of homogenization of 243.4^{0}C averaged over several trials. The range of visual error at the termination of Brownian Motion is in the range of 1^0 to 2^{0}C. This is insignificant when compared to those errors incorporated when temperature corrections are estimated graphically. For instance, only 25 MPa isochores are included in the plots of Potter. For depths in the area of 1470 m (deposition site at Axial Seamount) the corresponding pressure is:

FIGURE 4.3. Temperature correction as a function of pressure and the homogenization temperature for a) a 5 weight % NaCl solution and b) a 10 weight % NaCl solution (from Potter 1977).

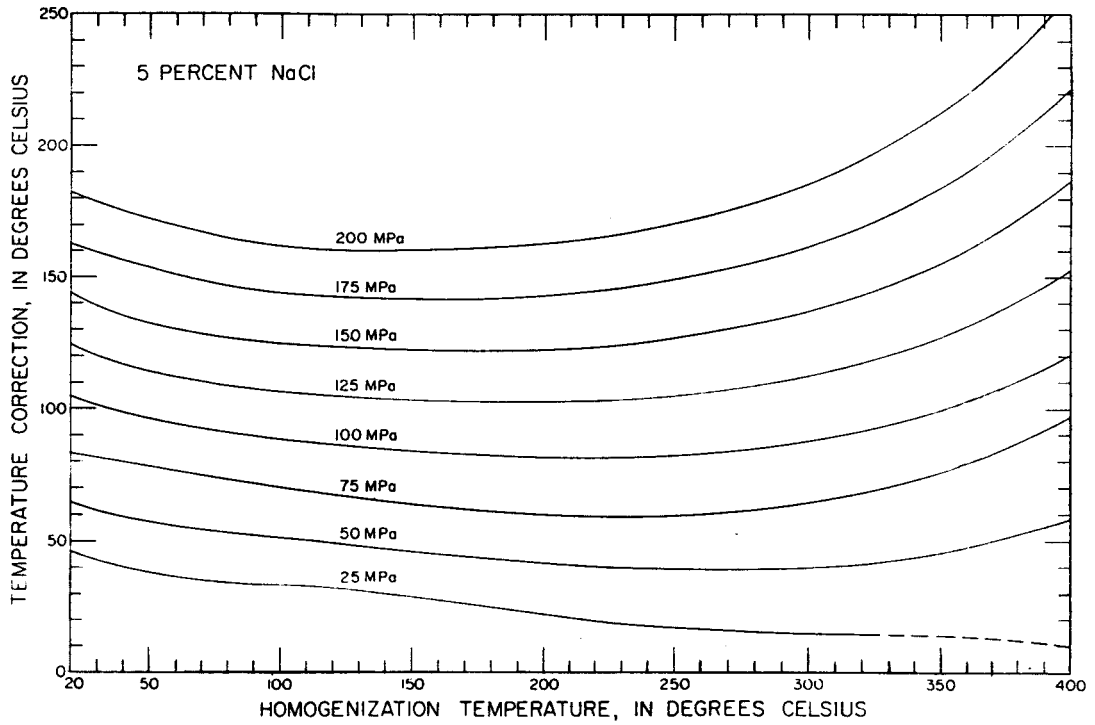
5 PERCENT NaCl
200 MPa
175 MPa
150 MPa
125 MPa
100 MPa
75 MPa
50 MPa
25 MPa
TEMPERATURE CORRECTION, IN DEGREES CELSIUS
HOMOGENIZATION TEMPERATURE, IN DEGREES CELSIUS
0
50
100
150
200
250
20
50
100
150
200
250
300
350
400

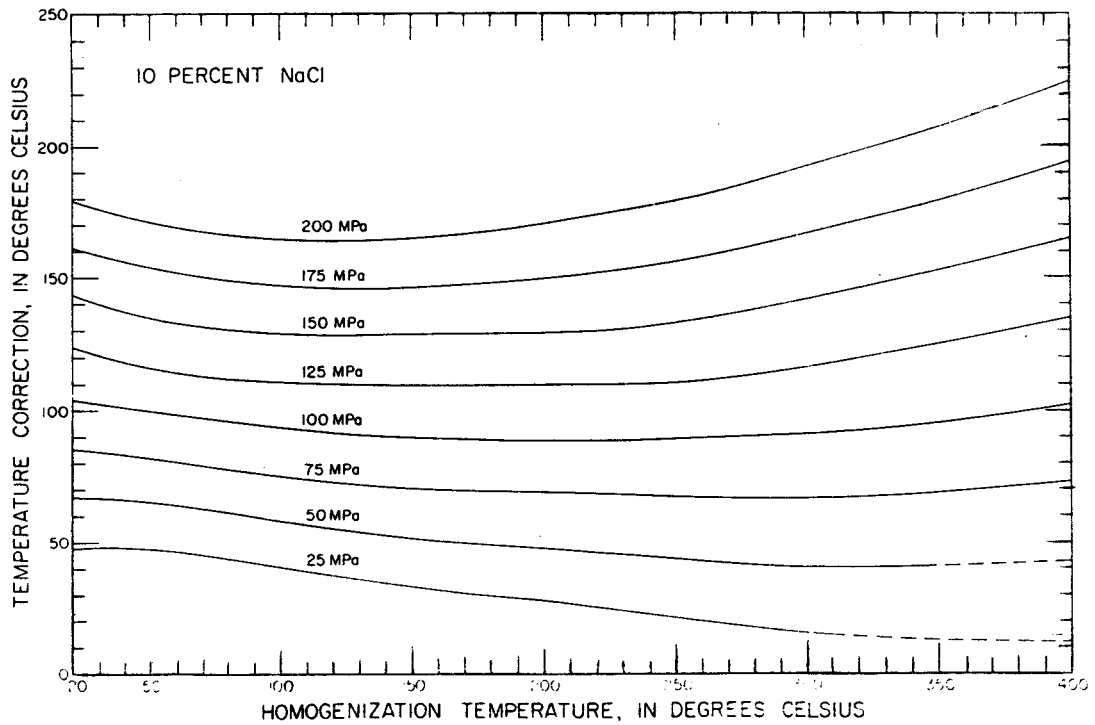
10 PERCENT NaCl
200 MPa
175 MPa
150 MPa
125 MPa
100 MPa
75 MPa
50 MPa
25 MPa
TEMPERATURE CORRECTION, IN DEGREES CELSIUS
HOMOGENIZATION TEMPERATURE, IN DEGREES CELSIUS
0
50
100
150
200
250

1470m * 3.28ft/m * 33.0ft/atm. * 1 atm./101.3 kPa * 1/1000

= 14.80 MPa

An estimate for this inclusion yields a required correction of ~10^{0}C for a 5 weight % NaCl solution and ~13^{0}C for a 10 weight % NaCl solution.

Pressure corrections for T_h, observed from measureable inclusions with compositions in the 5.6 to 7.0 weight percent range lie between ~9^{0}C and ~13^{0}C. The result is that pressure-corrected filling temperatures are +/- 9.0 to 13^{0}C off the calculated homogenization temperatures. Please see Table 4.3 for a complete list of T_h and pressure-corrections for measured inclusions.

Those inclusions having the highest observed homogenization temperatures (ie. Section XL-2A2, sphalerite grain 6, inclusion A, T_h = 269.4^{0}C, wt. % NaCl = 5.6222) at 14.80 MPa, require corrections of about 10^{0}C. An inclusion with a lower T_h (ie. Section XL-2A2, spalerite grain 7, inclusion A, T_h = 214.8^{0}C, wt. % NaCl = 6.65) at 14.80 MPa, requires a pressure-correction of ~13^{0}C. These examples are representative of the upper and lower limits of pressure corrections for the inclusions yielding accurate data. Several inclusions which yielded freezing point data could not be measured for T_h, and occasionally the reverse situation prevailed. Some inclusions which appeared useful for heating and/or freezing measurements on optical grounds

TABLE 4.3. Data for heating experiments from samples XL1720-2A and XL1720-2B. T_h = Homogenization temperature, SD = Standard deviation.

Sample XL1720-2B		Section XL-2B		
Grain#	Inclusion	T_h (Avg.^{0}C)	SD	Cor.^{0}C
1	A	243.73	0.63	+/- 12
Sample XL1720-2A		Section XL-2B		
Grain#	Inclusion	T_h (Avg.^{0}C)	SD	Cor.^{0}C
1	A	254.75	4.99	+/- 11
1	B	266.50	1.05	+/- 11
1 (Avg.)	-----	260.60	8.31	----
5	A	266.45	0.80	+/- 10
6	A	269.40	2.51	+/- 10
7	A	214.80	0.65	+/- 13
9	A	260.55	0.83	+/- 11
9	D	260.50	1.11	+/- 11
9 (Avg.)	-----	260.53	0.94	----
Sample (Avg.)	-----	256.13	18.88	----

could not be measured. Most of the problems could be traced to difficulties incurred with lighting conditions. Samples that were moved within the stage or removed completely and returned prior to the next measurement, could rarely be returned to the orientation and lighting conditions at which earlier measurements were performed. Such are a few of the problems involved with fluid inclusion studies.

Once again, reasonably sized fluid inclusions (>4-5 microns) in amorphous silica and barite were located and set-up for measurement. These inclusions yielded no homogenization data because leaking and decrepitation had resulted upon heating. Inclusions within recognizable wurtzite crystals were too small for analysis.

CHAPTER 5

DISCUSSION

Several distinct zones of hydrothermal activity are located along spreading centers of the Juan de Fuca Ridge in the northeast Pacific Ocean. Successive scientific investigations at a number of these sites, including sampling projects, has provided the necessary materials to begin thorough geologic studies on seafloor polymetallic sulphide deposits. The two locations studied here, Axial Seamount and Middle Valley, contain sulphide deposits that are largely similar to those at other Juan de Fuca Ridge vent sites, as well as to those areas of hydrothermal activity at other spreading centers in the eastern Pacific. Although the two sites have some similarities, they are quite different, the former representing a single active volcano caldera and the other a sediment-buried mid-ocean ridge.

Hydrothermal mineralization occurring within mounds at Middle Valley and along open fissures at Axial Seamount, reflect the morphological differences between the two sites. Middle Valley sulphides are the likely product of hydrothermal fluids which have reacted with the sedimentary pile on their way to the surface. The primary mineral phases are pyrrhotite, sphalerite, pyrite, marcasite, chalcopyrite/isocubanite, amorphous silica, and barite. The

dominance of pyrrhotite as opposed to pyrite can be related to fluid reaction with organic sedimentary material which results in low oxygen fugacities. Replacement of pyrrhotite by pyrite and marcasite is well developed in certain areas, as pyrite assumes the tabular form of the pyrrhotite grains. The replacement of pyrrhotite by other Fe sulphides was likely accompanied by an increase in oxygen fugacity as mixing with local seawater progressed. Wurtzite has been extensively inverted to sphalerite, as indicated by partial hexagonal outlines on the edges of sphalerite aggregates. The relative abundance of sphalerite compared to wurtzite is commonly considered a distinction between dead and active vents sites. Sphalerite occurs only as small quantities in the Middle Valley samples, when compared to non-sulphide phases. Chalcopyrite and isocubanite are commonly contained within the larger Zn sulphide grains, representing a typical exsolution pair. The high proportions of SiO_2 and Mg silicates represents the mixing of hydrothermal fluids with the hemipelagic sediment and the release of Mg from the structures of clay minerals and talc, and SiO_2 from amorphous silica. Barite is also quite common in the Middle Valley samples however, anhydrite was conspicuously absent. The retrograde solubility of anhydrite may have resulted in dissolution of this mineral with gradual cooling inside the deposit. These observations are consistent with decreased

concentrations of Zn, Cu, Pb, Cd, and Ag at Middle Valley, and higher concentrations of Ba, Mg, SiO_2, Fe, and Mo, compared to sulphides analysed from the East Pacific Rise and other Juan de Fuca Ridge sites, as discussed by Davis et al. (1987).

Axial Seamount sulphides are rich in sphalerite and wurtzite. Excellent wurtzite crystals are common and abundant in areas of open space. A few of these grains appear to be partially inverted to sphalerite. Sphalerite often occurs in coarse aggregates with individual grains usually containing some Cu-Fe sulphides. Dendritic growth patterns of Zn and Fe sulphides are another texture typical to zones of open space. Where pyrrhotite forms the early structure for encrustation in the Middle Valley suite of samples, colloform Zn and Fe sulphides perform a similar function at the Axial Seamount location. Very well developed concentric growth rings are common within the colloform precipitates. Barite and amorphous silica are less abundant in samples from Axial Seamount, as the bulk of the volume is occupied by the various sulphide minerals. Samples XL1720-2A and XL1720-2B have textures indicative of an active vent that is relatively mature in nature. Textural observations from the small sample available from Scott's Pinnacle, are in accord with those made by Hannington and Scott (1988) which indicate that the vent is immature. In general, the textural

features described for Axial Seamount samples, indicate that growth of sulphides are directly related to precipitation along open fissures.

Fluid inclusions are present in the minerals wurtzite, sphalerite, amorphous silica, and barite. Those inclusions within wurtzite are extremely minute, while those in the sphalerite, amorphous silica, and barite are considerably larger and contain two phases at room temperature. The few fluid inclusions visible in the Middle Valley samples, were far too small for measurement. Fluid inclusions in amorphous silica and barite, from samples XL1720-2A and XL1720-2B, were measured for both freezing point depression and homogenization temperatures however, a number of problems incurred during experimentation, including decrepitation and leakage upon heating, allowed no results to be obtained.

Freezing point depression was measured in approximately 35 two-phase fluid inclusions in coarse sphalerite. The range in final ice melting temperatures lay between $-3.45^{0}C$ and $-4.40^{0}C$. Subsequent calculations for composition yielded values in the range, 5.62 to 7.01 weight % NaCl. Sample XL1720-2A gave salinities from 5.62 to 6.65 weight % NaCl. Sample XL1720-2B revealed compositions in the 5.70 to 7.01 weight % NaCl range.

The compositions calculated are representive of fluids venting at sites within the caldera of Axial Seamount at the

time of main sulphide deposition. The fluids have been partially diluted by the circulation of ambient seawater which has mixed with the saline solutions near the surface of these deposits. Typical vent fluid compositions have been determined at Axial Seamount (CASM II 1985; Hannington and Scott 1988), at the Explorer Ridge (Tunnicliffe et al. 1986), at 21^{0}N along the East Pacific Rise (Edmond et al. 1982; Von Damm 1983), at the Galapagos Rift (Edmond et al. 1979a,b), and at Guaymas Basin (Von Damm 1983). These sulphide deposits show that increased dilution of end member fluids by seawater is occurring as the deposit matures. NaCl compositions from a silica-sulphide-sulphate spire sampled at Axial Seamount (Hannington and Scott 1988) are considerably less than those determined from samples in this study, which come from a higher temperature vent site, also located at Axial Seamount. The salinities determined in this study accurately reflect those expected from fluids in the 250^{0}C range.

Attempts were made to measure all of those inclusions that have been measured for salinity, for homogenization temperatures. Those that were reliable, showed T_H to lie in the range from 214.8^{0}C to 269.4^{0}C, averaging 250.9^{0}C. Corrections required to convert homogenization temperatures to trapping temperatures are from ~9.0^{0}C to ~13.0^{0}C. Fluid inclusions in sphalerite, from sample XL1720-2A, have homogenization temperatures that span the range given above.

This gives formation temperatures that lie above those for inclusions in wurtzite crystals at the CASM vent site (235^{0}C +/- 10^{0}C) (Hannington and Scott 1988), and below those for inclusions in Zn sulphide at 21^{0}N, along the East Pacific Rise (280^0 to 285^{0}C) (Styrt et al. 1981); (288^0 to 300^{0}C) (Le Bel et al. 1982). Sulphides were deposited at temperatures at least as high as 280^{0}C at the vent site considered in this thesis (PISCES vent), an average that falls within the range of formation temperatures for main stage sulphide deposition, determined at other similar vent sites. It appears that Zn sulphide deposition is confined to temperatures in the range 235^{0}C to 300^{0}C at this vent site and other vent sites as well. Active ridges buried beneath thick packages of sediments should deposit Zn sulphides at temperatures other than those described above, due to fluid equilibration with the sediment which results in different chemistry and resultingly different precipitation mechanisms. Concise fluid inclusion data from deposits such as those at Middle Valley and Guayamas Basin are not yet avaiable.

A significant number of inclusions in sample XL1720-2B, would not yield homogenization temperatures; however, those that did, lay in the same range. These temperatures are representative of the main stage of sulphide deposition for these Axial Seamount samples. Evidently, in future studies, it will be necessary to undertake fluid inclusion work armed

with a greater number of prepared sections.

Axial Seamount and Middle Valley are two very important sites for geological study. The pristine nature of the sulphide deposits that develope at ridge crest hydrothermal vents, offer a unique opportunity for thorough scientific investigation. Further detailed fluid inclusion microthermometric studies are required in order to grasp more fully the complex fluid history of these vent sites. The information gained in these studies together with mineralogical, isotopic, and geochemical analyses will eventually be used to formulate a concise description concerning the generation of these deposits.

REFERENCES

Adshead, J. D. (1987): Magnesium distribution and the nature of magnesian silicates in hydrothermally altered Juan de Fuca sediments. Amer. Geophys. Union Trans. Program Abstr. V. 68, p. 113.

Adshead, J. D., Bornhold, B. D., and Davis, E. E. (1986): Indurated deposits and possible plume bands in a hydrothermal mound, northeast Pacific. Curr. Res., Geol. Surv. Can. V. 86, pp. 737-748, 1986.

ASHES Expedition (1986): Pisces submersible exploration of a high-temperature vent field in the caldera of Axial Seamount, Juan de Fuca Ridge. EOS, Trans Amer. Geophys. Union V. 67, p. 1027.

Barton, P. B. (1978): Some ore textures involving sphalerite from the Furutobe Mine, Akita Prefecture, Japan. Mining Geology. V. 28, no. 45, p. 912.

CASM II (1985): Hydrothermal vents on an axis seamount of the Juan de Fuca Ridge. Nature V. 313, pp. 212-214.

Chen, C. T. A. and Marshall, W. L. (1982): Amorphous silica solubilities IV. Behaviour in pure water and aqueous sodium chloride, sodium sulphate, magnesium chloride, and magnesium sulphate solutions up to 350^{0}C. Geochim. Cosmochim. Acta 46, pp. 279-287.

Clague, D. A., and Bunch, J. E. (1976): Formation of ferro-basalt at East Pacific mid-ocean spreading centers. Jour. Geophys. Res. V. 81, pp. 4247-4256.

Clynne, M. A., and Potter, R. W. (1977): Freezing point depression of synthetic brines (abstr.). Geol. Soc. Amer. Abstr. Programs, V. 9, 930, pp. 250,289.

Davis, E. E., Goodfellow, W. D., Bornhold, B. D., Adshead, J. D., Blaise, B., Villinger, H., and Le Cheminant, G. M. (1987): Massive sulphides in a sedimented rift valley, northern Juan de Fuca Ridge. Earth and Planetary Science Letters, V. 82, pp. 49-61.

Eaby, J. S., and Clague, D. A. (1982): Preliminary description of basalt from the southern Juan de Fuca Ridge. U.S.G.S. Open-File Report 82-200C, 17 p.

Edmond, J. M., Measures, C.I., McDuff, R. E., Chan, L. H., Collier, R., Grant, B., Gordon, L. I., and Corliss, J. B. (1979a): Ridge crest hydorthermal activity and the balances of the major and minor elements in the ocean. The Galapagos data. Earth and Planetary Science Letters, V. 46, pp. 1-18.

Edmond, J. M., Measures, C. I., Mangum, B., Grant, B., Sclater, F. R., Collier, R., Hudson, A., Gordon, L. I., and Corliss, J. B. (1979b): On the formation of metal-rich deposits at ridge crests. Earth and Planetary Science Letters, V. 46, pp.19-30.

Edmond, J. M., Von Damm, K. L., McDuff, R. E., and Measures, C. I. (1982): Chemistry of hot springs on the East Pacific Rise and their effluent dispersal. Nature, V. 297, pp. 187-191.

Goodfellow, W. D., and Blaise, B. (1988): Sulphide formation and hydrothermal alteration of hemipelagic sediment in Middle Valley, northern Juan de Fuca Ridge. Canadian Mineralogist, V. 26, pp. 675-696.

Graham, U. M., Bluth, G. J., and Ohmoto, H. (1988): Sulphide-sulphate chimneys on the East Pacific Rise, 11^0 and 13^0 latitudes. Part II: sulfur isotopes. Canadian Mineralogist V. 26, pp.487-504.

Grasty, R. L., Smith, C. W., Franklin, J. M., and Jonasson, I. R. (1988): Radioactive orphans in barite-rich chimneys, Axial Caldera, Juan de Fuca Ridge. Canadian Mineralogist V. 26, pp. 627-636.

Hammond, S.R., Karsten, J., Davis, E. E., Currie, R., and Malahoff, A. (1983): Bathymetric and hydrothermal characterization of the northernmost Juan de Fuca Ridge. EOS. Trans. America Geophys. Union. V. 64, p. 853.

Hannington, M. D., (1986): Geology, Mineralogy and Geochemistry of a Silica-Sulphate-Sulphide Deposit; Axial Seamount, N.E. Pacific Ocean. M.Sc. Thesis, Univ. of Toronto, Toronto, Ontario.

Hannington, M. D., and Peter, J. M., and Scott, S. D. (1986): Gold in sea-floor polymetallic sulphide deposits. Econ. Geol. V. 81, pp. 1867-1883.

Hannington, M. D., and Scott, S. D. (1988): Mineralogy and Geochemistry of a hydrothermal silica-sulphide-sulphate spire in the caldera of Axial Seamount, Juan de Fuca Ridge. Canadian Mineralogist, V. 26, pp. 603-625.

Haymon, R. M., and Kastner, M. (1981): Hot spring deposits on the East Pacific Rise at 21^{0}N: preliminary description of mineralogy and genesis. Earth and Planetary Science Letters, V. 53, pp. 363-381.

Hekinian, R., and Fouquet, Y. (1985): Volcanism and metallogenesis of axial and offaxial structures on the East Pacific Rise near 13^{0}N. Econ. Geol. V. 80, pp. 221-249.

Short course in Fluid Inclusions: Applications to Petrology. In: Mineralogical Assoc. of Canada (Hollister, L. S. and Crawford, M. L. ed.) V. 6, pp. 79-87, 94, 95.

Juniper, S. K., and Fouquet, Y. (1988): Filimentous iron-silica deposits from modern and ancient hydrothermal sites. Canadian Mineralogist, V. 26, pp. 859-869.

Kingston, M. J., Delaney, J. R., and Johnson, H. P. (1983): Sulphide deposits from the Juan de Fuca Ridge at 45^{0}57'N, 129^{0}06'W. Oceans V. 83, Aug.29-Sept.1, 1983, San Francisco, Proc., v II. pp. 811-815.

Koski, R. A., Normark, W. R., Morton, J. L., and Delaney, J. R. (1982): Metal sulphide deposits on the Juan de Fuca Ridge. Oceanus, V. 25, pp. 42-48.

Koski, R. A., Clague, D. A., Oudin, E. (1984): Mineralogy and chemistry of massive sulphide deposits from the Juan de Fuca Ridge. Geol. Soc. America Bull., V. 95, pp. 930-945.

Le Bel, L., and Oudin, E. (1982): Fluid inclusion studies of deep-sea hydrothermal massive sulphide deposits on the East Pacific Rise near 21^{0}N. Chemical Geology, V. 37, pp. 129-136.

Malahoff, A., McMurtry, G. M., Hammond, S., and Embley, R. (1984): EOS, Trans. Amer. Geophys. Union. V. 65, p. 1112.

Malahoff, A., (1985): Hydrothermal vents and polymetallic sulphides of the Galapagos and Gorda/Juan de Fuca Ridge sytems and of sudmarine volcanoes. In: Hydrothermal vents of the Eastern Pacific: An overview (M. L. Jones. ed.). Bull. Geol. Soc. Wash. V. 6, pp. 19-41.

MERGE (1984): Regional setting and character of a hydrothermal field/sulphide deposit on the Endeavor Segment of the Juan de Fuca Ridge. EOS, Trans. Amer. Geophys. Union. V. 65 p. 1111.

Normark, W. R., Morton, J. L., Koski, R. A., Clague, D. A., and Delaney, J. R. (1983): Active hydrothermal vents and sulphide deposits on the southern Juan de Fuca Ridge. Geology, V. 11, pp. 158-163.

Normark, W. R., Lupton, J. E., Murray, J. W., Delaney, J. R., Johnson, H. P., Koski, R. A., Clague, D. A., and Morton, J. L. (1982): Polymetallic sulphide deposits and water-column of active hydrothermal vents on the southern Juan de Fuca Ridge. Mar. Tech. Soc. Jour. V. 16, pp. 46-53.

Oudin, E., (1981): A mineralogical and Geochemical study of seafloor polymetallic sulphide deposits on the East Pacific Rise at 21^0N. Bur. Recherches Geol. Min. Doc., no. 25, 241 p.

Oudin, E. (1983a): Hydrothermal sulphide deposits of the East Pacific Rise at 21^0N. Part I: Descriptive mineralogy. Mar. Geol. V. 4, pp. 39-72.

Paradis, S., Jonasson, I. R., Le Cheminant, G. M., and Watkinson, D. H. (1988): Two zinc-rich chimneys from the Plume Site, southern Juan de Fuca Ridge. Canadian Mineralogist. V. 26, pp.637-654.

Picot, P., and Fevrier, M. (1980): A mineralogical study of sulphide deposits in the Gulf of California. (CYAMEX campaign). Bur. Recherches Geol. Min. Doc. no. 20.

Potter, R. W. (1977): Pressure corrections for fluid-inclusion homogenization temperatures based on the volumetric properties of the system NaCl-H_2O. U.S.G.S. Jour. Res. V. 5, no. 5, pp. 603-607.

Potter, R., Clynne, M. A., and Brown, D. L. (1978): Freezing point depression of aqueous sodium chloride solutions. Econ. Geol. V. 73, pp. 284-285.

Roedder, E. (1984): Reviews in mineralogy: Fluid inclusions. Reviews in Mineralogy. V. 12, pp. 13-25, 31-35, 59-66, 221-237, 252-264.

Scott, S. D., and Barnes, H. L. (1972): Sphalerite-wurtzite equilibria and stoichiometry. Geochim. Cosmochim. Acta 36, pp. 1275-1295.

Scott, S.D., (1983): Chemical behaviour of sphalerite and arsenopyrite in hydrothermal and metamorphic enviroments. Mineral. Mag. V. 47, pp. 427-435.

Scott, S. D. (1985): Seafloor polymetallic sulphide deposits: modern and ancient. Mar. Mining. V. 5, pp. 191-212.

Shepherd, T., Rankin, A. H., and Alderton, D. H. M. (1985): A practical Guide to Fluid Inclusion Studies. pp. 63-68, 72-74, 94-113, 124-129.

Styrt, M. M., Brackman, A. J., Holland, H. D., Clark, B. C., Pusutha-Arnond, V., Eldridge, C. S., and Ohmoto, H. (1981): The mineralogy and the isotopic composition of sulphur in hydrothermal sulphide/sulphate deposits on the East Pacific Rise, 21^0N latitude. Earth and Planetary Science Letters. V. 53, pp. 382-390.

Tivey, M. K., and Delaney, J. R. (1986): Growth of large sulphide structures on the Endeavor Segment of the Juan de Fuca Ridge. Earth and Planetary Science Letters. V. 77, pp. 303-317.

Tunnicliffe, V., Botros, M., DeBurgh, M. E., Dinet, A., Johnson, H. P., Juniper, S. K., and McDuff, R. (1986): Hydrothermal vents of Explorer Ridge, Northeast Pacific. Deep-Sea Res. V. 33, pp. 401-412.

U.S.G.S. Juan de Fuca Study Group (1986): Submarine fissure eruptions and hydrothermal vents on the southern Juan de Fuca Ridge: Preliminary observation from the submersible Alvin. Geology. V. 14, pp. 823-827.

Villinger, H. and Davis, E. E. (1986): Hydrothermal regime of a sedimented rift valley, northern Juan de Fuca Ridge. EOS Trans. America Geophys. Union. V. 67, p. 1232.

Vogt, P. R., and Byerly, G. R. (1976): Magnetic anomalies and basalt composition in the Juan de Fuca-Gorda ridge area. Earth and Planetary Science Letters. V. 33, pp. 185-207.

Von Damm, K. L. (1983): Chemistry of submarine hydrothermal solutions at 21^0N, East Pacific Rise and Guayamas Basin, Gulf of California, Ph.D. dissertation, 240 pp., Mass. Inst. of Technol./Woods Hole Oceanogr. Inst. Joint Program in Oceanogr.